Technische Universität München

Lehrstuhl für Technische Chemie II

Hollow sphere structures for the emission limitation

of internal combustion engines

Wolfgang Kaltner

Vollständiger Abdruck der von der Fakultät für Chemie der Technischen Universität München

zur Erlangung des akademischen Grades eines

Doktors der Naturwissenschaften (Dr.rer.nat.)

genehmigten Dissertation.

Vorsitzender: Univ.-Prof. Dr. K.-O. Hinrichsen

Prüfer der Dissertation:

1. Univ.-Prof. Dr. J. A. Lercher
2. Univ.-Prof. Dr. U. K. Heiz

Die Dissertation wurde am 14.05.2008 bei der Technischen Universität München eingereicht und durch die Fakultät für Chemie am 18.06.2008 angenommen.

ACKNOWLEDGEMENTS

TABLE OF CONTENTS

Chapter 1

1   INTRODUCTION

Motor vehicles emit significant quantities of air pollutions (see fig. 1), which influence the environment, climate and health negatively. The introduction of regulations to control and limit these emissions led to the development of exhaust gas aftertreatment systems.
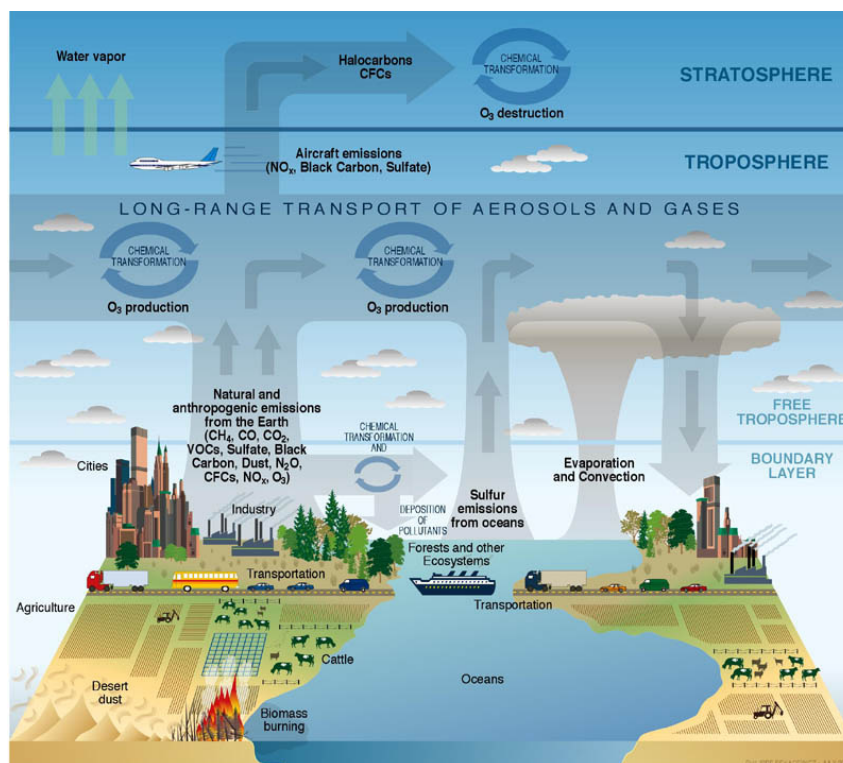
Figure 1: Sources and spreading of air pollutants in the atmosphere[1]

1.1 VEHICLE EMISSIONS AND ENVIRONMENTAL & HEALTH PROBLEMS

Major air pollutants emitted by cars and other vehicles in the transport sector, like aircraft, trains and ships are carbon monoxide (CO), particulate matter (PM), sulphur oxides (SO_x), nitrogen oxides (NO_x), hydrocarbons (HC) and carbon dioxide (CO_2). The negative influence of nitrogen oxide (NO_x) emissions to the environment result from their contributions to acid rain, smog and the greenhouse effect (especially N_2O) and moreover to the depletion of the earth protective ozone layer. Nitrogen oxides produce several negative health effects through NO_x intrusion in the respiratory system. Carbon dioxide (CO) is a tasteless, odourless and colourless gas produced through the incomplete combustion of carbon-based

---

[1] Source: http://www.climatescience.gov/Library/stratplan2003/final/graphics/images/SciStratFig3-1.jpj

fuels. CO enters the bloodstream through the lungs; blocks the binding of O_2 to haemoglobin and that reduces the delivery of oxygen to the organs. Hydrocarbons (HC) are known to be involved in the formation of ozone as a photochemical precursor. HC derivates, as for example benzene, are toxic to the human body and extremely carcinogen. Particulate matter (PM) is the term for the mixture of solid particles and liquid droplets found in the air [1]. PM includes dust, dirt, soot, smoke and liquid droplets emitted from motor vehicles or formed by condensation or transportation of emitted exhaust gases in the atmosphere (see fig. 2). The small particles (less than 2.5 μm in diameter) can penetrate the respiratory defence system and can be linked to a series of health problems, like chronic bronchitis, premature death and even lung cancer. Besides CH_4 and N_2O, carbon dioxide (CO_2) is known to be the major greenhouse gas. In the most countries, over 90 % of the global warming potential of the direct acting greenhouse gases from transportation sector comes from CO_2 [2].
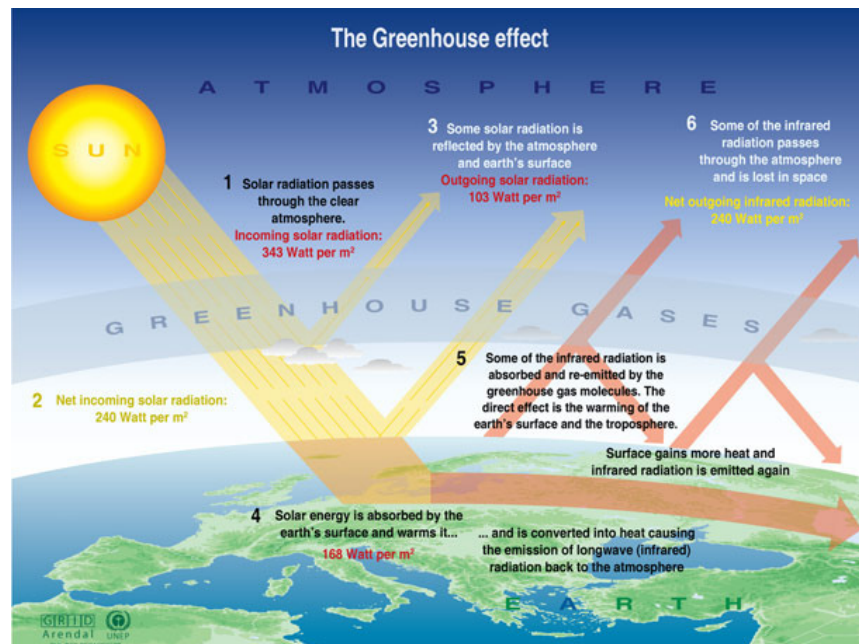
Figure 2: The influence of Greenhouse Gases on the atmosphere[2]

---

[2] Sources: Okanagan university college in Canada, Department of geography; University of Oxford, school of geography; United States Environmental Protection Agency (EPA)

The transportation sector is responsible for approximately 17 % of global CO_2 emissions and these emissions are still increasing due to the rapid increasing numbers of vehicles [3].

1.2 EMISSION LEGISLATION

The EU has adopted strict new limits on pollutant emissions from diesel and petrol cars, limiting in particular nitrogen oxides (NOx) and particulate matter (PM), which pose the most serious health and environmental problems. Fuel exhausts have an impact on air quality and human health, especially on in urban areas where traffic is dense. The EURO 5 standards for cars will further restrict emissions, from both petrol and diesel cars, of carbon monoxide (CO), hydrocarbons (HC), oxides of nitrogen (NOx) and particulate matter (PM) [4]. The tighter standards will apply as of September 2009 for new models of cars and in January 2011 for all new cars (see fig 3). The new directive will also close the loop-holes, under the Euro 4 Directive, for heavy sports utility vehicles (SUVs) and cars with four-wheel drives above 2500 kg. Emissions of the highly noxious pollutants known as nitrogen oxides and particulate matter from diesel vehicles are currently four to five times higher than for petrol vehicles. The Euro 5 Directive aims to make diesel cars catch-up - although not completely. The Euro 5 limits will reduce emissions of particulates from diesel cars by 80 % compared to Euro 4.
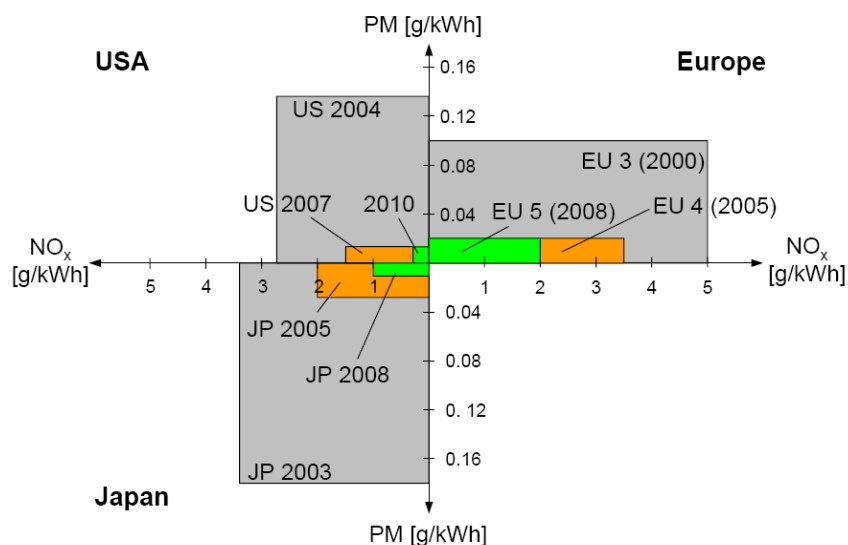
Figure 3: Comparison of NO$_x$ and PM limits in Europe, US and Japan

They will however be more lenient as regards NO_x emissions, which will only have to be cut from 250 mg/km to 180 mg/km – against a current 70 mg/km for petrol cars. This leniency for diesel vehicles contrasts with legislation in the United States, which is "fuel-neutral". However, it is worth mentioning that diesel cars represent half of all cars in the EU, whereas they represent less than 5 % of those in the US. To prepare for new standards, carmakers are working on technologies to optimize diesel engines. The quantity and composition of emissions vary depending on several technical factors, including the quality of diesel fuel used,; the type of engine and the engine tuning; the workload demand on the engine, etc. The tightening of vehicle standards is closely linked to fuel quality improvements. In some cases, fuel modifications are necessary to allow the introduction of new technologies that are needed in order to meet the tighter emission standards. For example, the adoption of EURO 1 standards for gasoline vehicles required the development of unleaded gasoline. The emission standards are always technology-neutral, which means that carmakers can use the technology of their choice to reduce emissions. At the time of their adoption, the EURO 4 standards were believed to require expensive particulate filters to be fitted into diesel cars. But progress in the engine technology made it possible to meet the EURO 4 particulate matter limit (25 mg/km) on most cars using advanced in-cylinder techniques and the diesel oxidation catalyst (DOC), without the need for a PM filter. Current EURO 5 proposals, however, given current technology, can only be achieved by fitting expensive filters to exhaust tubes. Member states are free to introduce fiscal incentives to reduce emissions beyond EURO 4 emission standards which have applied since January 2005. Germany, for instance, has a tax exemption of about € 600 for new cars bought if PM emissions are under 0.0085 mg/km. Similar incentives are proposed in France, Austria and the Netherlands.

In January 2005, the Commission issued a guidance document for the purposes of countries wishing to go beyond Euro 4. Japan and the US have adopted similar legislation to the Euro emission standards. Emerging countries in Asia, Africa and South America are

also gradually adopting legislation on emission standards and fuel requirements in order to avoid serious air pollution problems linked to the growing numbers of automobiles on their roads. In 2005, Indonesia, Nepal, Philippines, and Bangladesh remained under Euro 1 standards. In Russia Euro III standards started in the beginning of 2008. 2010 the standards will be upgraded to Euro IV and 2014 to Euro V. India has announced Euro III standards 2005, which will be upgraded to Euro IV until 2010 [5]. China enacted its first emission controls on automobiles in 2000, equivalent to Euro I standard. They were upgraded again in 2005 to Euro II. More stringent emission standard, equivalent to Euro 3 went into effect in 2007 [6]. Plans are for Euro IV standards to take effect in 2010. Beijing introduced the Euro IV standard in advance already in the beginning of 2008 [7].

Beyond EURO 5, the EU institutions have agreed on introducing longer-term limits, under a EURO 6 stage that has been adopted at the same time as EURO 5 (see table 1), but will enter into force five years later. EURO 6 will set significantly lower emission limits for NOx emissions from diesel engine cars. [8, 9]

Table 1: EU Emission Standards [10, 11]

Emission Standard	CO [mg/km]		PM [mg/km]		HC + NOx [mg/km]		NOx [mg/km]		HC [mg/km]	
	Diesel	Petrol	Diesel	Petrol	Diesel	Petrol	Diesel	Petrol	Diesel	Petrol
Euro 2 (1996)	1000	2200	80-100		700-900	500				
Euro 3 (2000)	640	2300	50		560		500	150		200
Euro 4 (2005)	500	1000	25		300		250	80		100
Euro 5 (2009)	500	1000	5	5	230		180	60		100
Euro 6 (2014)	500	1000	5	5	170		80	60		100

In the United States, emission standards are managed by the Environmental Protection Agency. Some of the strictest standards in the world are enforced in California. Currently, vehicles sold in the United States must meet "Tier II" standards that went into effect in 2004. "Tier II" standards are being phased in, which will be finished 2009. Within the Tier II ranking there is a subranking ranging from BIN 1-10, with 1 (Zero Emission Vehicle) being the cleanest and 10 being the dirtiest. [12]

1.3 POLITICAL INFLUENCES

The European Commission is working on future policy options for the car industry providing a long term strategy. A high level of environmental protection in the European Union and contribution to reach the EU's Kyoto targets has to be achieved. Progress is needed to reach the long-standing EU objective of an average new car fleet emission of 120 g CO_2/km until 2012 (compare emissions 2008 in fig. 4), focusing on mandatory reductions to reach the objective of 130 g CO_2/km on average for the new car fleet through improvements in vehicle motor technology, and a further reduction of 10 g CO_2/km, or equivalent if technically necessary, by other technological improvements and by increased use of bio-fuels. New car models entering the market must be approved by a certified type approval institution in the Member States on a mandatory basis. [13]
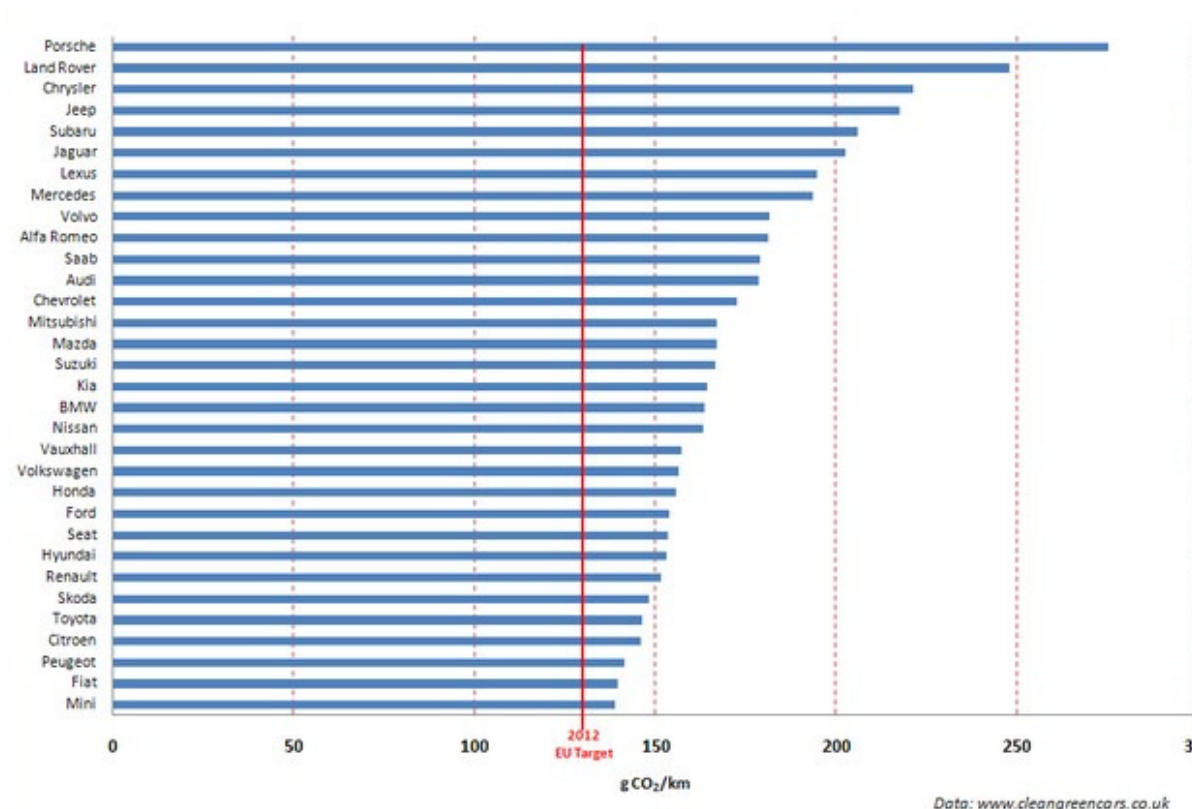
Figure 4: Average Sales-weighted CO$_2$ Emissions per vehicle by manufacturer in UK 2008

2006, the German government has enacted the decree according to EU specifications that low-emission vehicles are marked. This decree should help to reduce the particulate matter exposure in cities, which is currently too high in many cities. The decree aims to label all vehicles nationwide according to their particulate matter emissions. Furthermore, a new traffic sign "pollution-free zone" (Umweltzone) will be introduced to mark the restricted areas. [14]

The emission labels are available in three colours according to the emission group, which can be found in the vehicle registration certificate (see table 2).

Table 2: Emission Groups with according numbers out of the vehicle registration certificate

Emission group	Green (4)	Yellow (3)	Red (2)
Otto Engine			
Cars according to EU class M_1	01, 02, 14, 16, 18-70, 71-75, 77		
Diesel Engine			
Cars according to EU class M_1	32, 33, 38, 39, 43, 53-70, 73-75, PM 5	30, 31, 36, 36, 42, 44-52, 72	25-29, 35, 41, 71
Cars according to EU class M_1 + refitted particulate filter	PM 1: 27, 49-52 PM 2: 30, 31, 36, 37, 42, 44-48, 67-70 PM 3: 32, 33, 38, 39, 43, 53-66 PM 4: 62-70	PM 0: 28, 29 PM 1: 14, 16, 18, 31, 22, 25-29, 34, 35, 40, 41, 71, 77	PM 01: 19, 20, 23, 24 PM 0: 14, 16, 18, 21, 25-29, 34, 35, 40, 71, 77

The green emission label for emission group 4 is for cars with low emissions. The yellow emission label is for cars belonging to emission group 3. The red label is for cars in the emission group 2. Cars in the emission group 1, gasoline engines without catalyst or old diesel engines, are not labelled and can not enter pollution-free zones in general. Vehicles with green labels are allowed to enter the pollution-free zones without restrictions. Yellow and red labelled cars can be banned from these zones depending on the actual or permanent concentration of particulate matter. Several cities in Germany have active (beginning of 2008) pollution-free zones implemented, e.g. Berlin, Dortmund, Hannover, Köln, Mannheim, and Stuttgart. Further cities will follow, e.g. Augsburg, München, and Heidelberg. [15]

1.4 STATE OF SCIENCE AND TECHNOLOGY

The European Union implemented 1993 the Auto/Öl-Programm (car/oil program) as initiative for the further reduction of exhaust emissions. Based on the requirements for air purity of the World Health Organization (WHO) in highly populated areas, which will be due 2010. Various engine concepts and exhaust gas treatment systems (see fig. 5) are developed for the achievement of the objectives. [16]

European-spec Model Year 2006 E-Class shown with BLUETEC® technology.
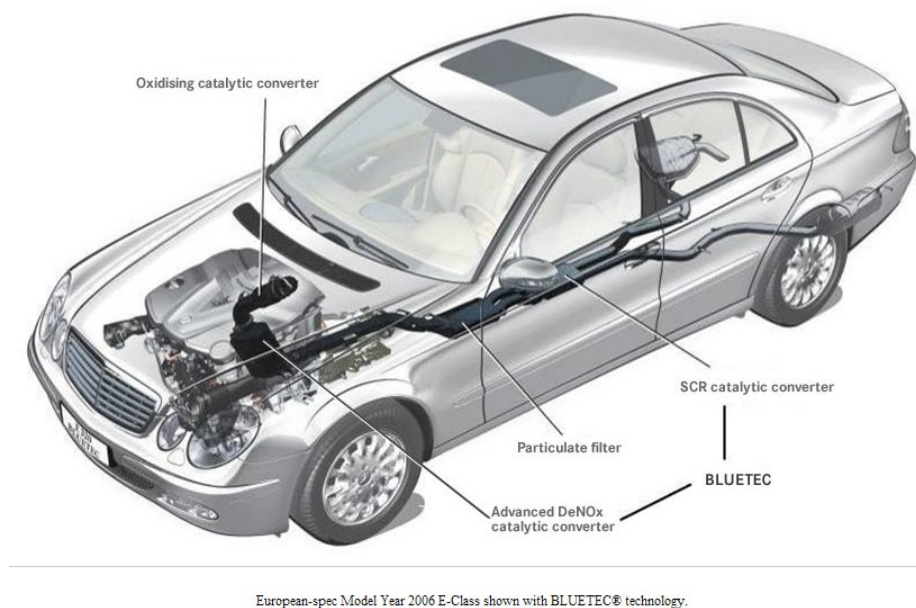
Figure 5: Mercedes E-Class Bluetec technology[3]

Nowadays, the diesel engine is the least fuel consuming concept on the motor side. Implementation of new technologies, like the high-pressure fuel-injection pump, increased the efficiency and reduced the exhaust emissions. These so-called inner-motor solutions for the emission limitation are limited because the formation of emissions on one hand and the combustion conditions on the other hand require contrary demands for the minimization of nitric oxides and particulate matter. Exhaust gas treatment systems can solve this conflict of objectives. In the process two basic tendencies for optimization are considered. The first is based on the reduction of nitrogen oxides with a particulate filter whereas a DeNOx catalyst

---

[3] http://www.mercedes-benz.de

reduces the particles in the second alternative. Problems in these systems lead to intensified research on combined DeNOx-particulate filter systems.

1.4.1 Diesel Particulate filter

Particulate filters are at the moment the most effective method to reduce the particle emissions of diesel engines [17-19]. Soot particles are hold back up to 99 % and more than 90 % of total particles are hold back by a modern particulate filter nearly independent on particle size distribution. Without taking further action, the filter would be blocked with time. The technical challenge is the development of reliable regeneration methods, which is dominated by exhaust gas temperature (raising the temperature above 600 °C is required) and to a lower extent also by pressure drop, rest oxygen content, filtration speed, and space velocity. Currently two different principles are possible for the regeneration. On one side are active regeneration methods like fuel post-injection, combustion-controlled regeneration or electric heating. On the other side passive systems by means of catalytic active substances such as fuel-additives (see the following equations) (based on cerium or iron reduce the soot ignition temperature) or catalytic active coatings of filter elements. Modern and reliable operating particulate filter systems are utilized in combined regeneration systems based on different materials like cordierite filters, SiC filters and metal based filters (see fig. 6) nowadays [20-23].

The following equations describe the chemical reactions in the Diesel particulate filter.

$$C + 2CeO_2 \rightleftharpoons Ce_2O_3 + CO$$

$$2\,CO + O_2 \rightleftharpoons 2\,CO_2$$

$$C + 2NO_2 \rightleftharpoons CO_2 + 2NO$$

$$C + O_2 \rightleftharpoons CO_2$$
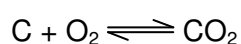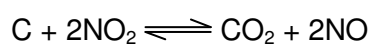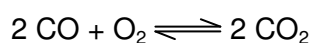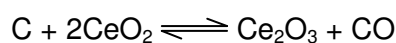
Depending on the choice of filter system an additional oxidation catalyst is used to generate the necessary exothermic energy for the regeneration of the wall-flow filters.
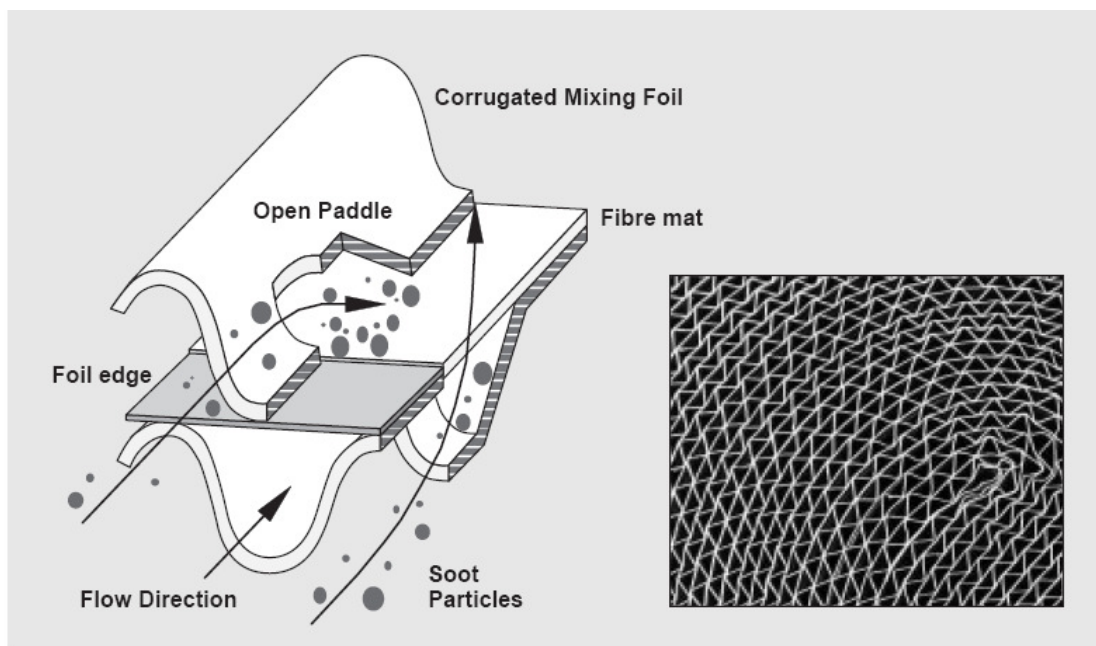
Figure 6: Principle of the PM Filter Catalyst

1.4.2 DeNOx process

The treatment of nitrogen oxides is rather difficult for Diesel engines due to their lean-burn ($\lambda > 1$) conditions. For this reason, reduction for the removal of NO_x, which is used in three-way-catalysts, can not be accomplished. DeNOx catalysts are applied with two different concepts: SCR-catalyst and NOx-storage-catalyst [24].

The SCR-catalyst converts the undesired nitrogen oxides to nitrogen and water with the addition of a selective reducing agent (ammonia). This technique is mainly applied in light duty vehicles. For passenger cars, the highly toxic ammonia is replaced by materials that release ammonia under a heating procedure, e.g. urea. The catalyst structure consists of coated honeycombs made of titania or vanadia, which achieve NO_x-conversions up to 90 %. The principal chemical reactions are:

$$4NO + 4NH_3 + O_2 \rightleftharpoons 4N_2 + 6H_2O$$

$$NO + NO_2 + 2NH_3 \rightleftharpoons 2N_2 + 3H_2O$$
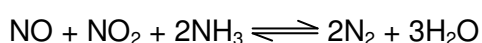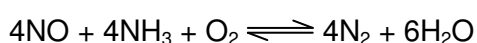
In a highly efficient SCR system there is a risk of ammonia slip behind the SCR catalyst in trucks or stationary applications. This can be prevented by fitting an oxidation catalyst

behind the SCR catalyst or by applying an oxidation coating to the rear part of the SCR catalyst in order to oxidize the NH_3 [25].

The NO_x storage-catalyst principle is based on a two step procedure, storage and regeneration [26]. Under normal, running engine, conditions, reactions take place with the result of storing NO_x in the catalyst. If the catalyst storage capacity is full, the engine control switches for a short time to rich conditions, in order to reduce the NO_x to nitrogen, similar to the three-way-catalyst. The catalyst is active between 250 – 450 °C [27]. Figure 7 shows an overview of regeneration concepts. The CRT® system is the most widely used system comprising an oxidation catalyst followed by a diesel particulate filter.
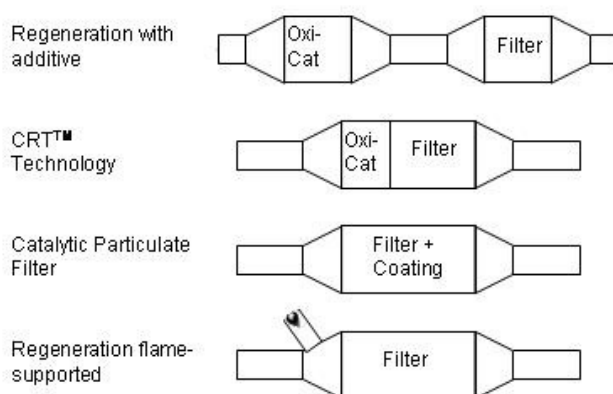
Figure 7: Overview of Regeneration Concepts

However, due the additional fuel demand for the regeneration and the irreversible deactivation of the catalyst in presence of S containing fuels this technology is currently not further developed.

1.4.3 Diesel oxidation catalyst

Oxidation catalysts are used to reduce HC and CO emissions [28, 29]. In addition, NO is oxidized to form NO_2 at a temperature between 200 and 450 °C.

NO_2 can be used to burn particulates or to improve the low-temperature efficiency (180 – 350 °C) of zeolite SCR catalysts. Oxidation catalysts have either Pt or a Pt/Pd coating [30] depending on the temperature load. The following chemical reactions take place:

$$2NO + O_2 \rightleftharpoons 2NO_2$$

$$2CO + O_2 \rightleftharpoons 2CO_2$$

$$C_mH_n + (m+n/4)\,O_2 \rightleftharpoons mCO_2 + n/2\,H_2O$$
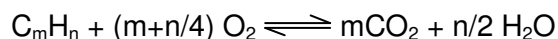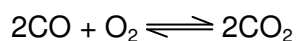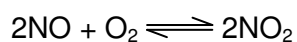
Diesel engine manufacturers have preferred to use parallel channeled flow-trough ceramic honeycomb monoliths to support the catalytic washcoat, thereby avoiding the soot plugging problems and regeneration requirements associated with the wall-flow diesel particulate filter [31, 32]. These diesel oxidation catalysts resemble the conventional catalytic converters for gasoline fired engines with some significant variation to the catalyst composition, based on noble metals, so as to optimize the catalyst activity under lean conditions [33]. To improve the catalyst performance there is a continuous drive towards higher operating temperature, thinner components and alternative geometries offering large surface area to volume ratios while maintaining acceptable component live is mandatory. This has led to a number of materials development strategies, including alternative substrate geometries, modifications to the alloy composition, both through the addition of multiple reactive elements and through the close control of trace element additions. Various support structures are available, including honeycomb catalyst substrates, cordierite wall flow filters, filters, silicon carbide wall flow filters and metallic wall flow filters. Furthermore zirconia ceramic foam filters and silicon carbide ceramic foam filters with extreme low weight are available. The reverse structures, metal sphere structures, in particular hollow sphere structures because of the reduced weight, are a promising alternative due to their stable structure.

14

1.5 REFERENCES

[1] A.Y. Watson, in: Diesel Exhaust: A Critical Analysis, Health Effects Institute, 1995, p.139

[2] Second Assessment Report of the Intergovernmental Panel on Climate Change (IPCC), "Climate Change 1995: The Science of Climate Change", ed. J.T. Houghton, Cambridge University Press, Cambridge, 1996

[3] G.M. Green, Diesel Emissions and Lung Cancer: Epidemiology and Quantitive Risk Assessment, Health Effects Institute, 1999

[4] http://en.wikipedia.org/wiki/European-emission standards

[5] www.siamindia.com/scripts/emission-standards.aspx

[6] http://English.cri.cn/2946/2007/07/176@244647.htm China launches tougher auto emission standard

[7] http://www.automotiveworld.com/AEM/content.asp?contentid=65589 China: Beijing launches Euro 4 standards

[8] http://www.euractiv.com/en/transport/euro-5-emissions-standards-cars/article-133325

[9] R. Thom, Emission and Fuel Economy Regulations for Passenger Cars in Europe, USA and Japan, Seminar Emission Control 2002, Dresden, June 10-11, 2002, p.13

[10] http://www.euractiv.com/en/transport/euro-5-emissions-standards-cars/article-133325

[11] http://dieselnet.com/standards/eu/ld.php

[12] http://www.dieselnet.com/standards/us/ld.php

[13] ACEA, Brochure: Reducing CO_2 Emissions from Cars (2008)

[14] http://www.umweltbundesamt.de/umweltzonen/index.htm

[15] http://osiris.uba.de/Website/umweltzonen/index.htm

[16] Bulletin EU 6-1996 (1996)

[17] A. Schaefer-Sindlinger, Topics in Catalysis 42-43 (2007) 307

[18] O. Salvat, SAE Technical Paper No. 2000-01-0473, 2000.

[19] J. Gieshoff, SAE Technical Paper No. 2001-01-0907, 2001.

[20] S. Hashimoto, SAE Technical Paper No. 2002-01-0322, 2002.

[21] A. Schaefer-Sindlinger, MTZ Motortechnische Zeitschrift, 3 (2003), p. 200.

[22] S. Ichikawa, SAE Technical Paper No. 2003-01-0380, 2003.

[23] S. Yamaguchi, SAE Technical Paper No. 2005-01-0666, 2005.

[24] J. Gieshoff, SAE 2000-01-0189, 2000

[25] R. Brück, SAE 2001-01-1950, 2001

[26] W. Strehlau, SAE 962490

[27] M.S. Brogan, SAE 952490

[28] B.J. Cooper, Platin. Met. Rev. 35 (1991) 178

[29] M. Horiuchi, SAE 900600, 1990

[30] R.J. Farrauto, Appl. Catal. B Environmental 10 (1996) 29

[31] R.M. Heck, Catalytic Air Pollution Control: Commercial Technology, Van Nostrand Reinhold, NY, 1995, Chap. 7, p 113

[32] R.J. Farrauto, Applied Catalysis B: Environmental 10 (1996), 29-51

[33] D. Fino, V. Specchia, Powder Technology 180 (2007) 64-73

Chapter 2

2   Scope and objectives of the thesis

2.1 OBJECTIVE OF THE PROJECT

Main parts of the experimental work of this thesis were carried out within the BMBF-Project "Hohlkugelstrukturen zur Verminderung von Emissionen bei Verbrennungs-kraftmaschinen" ("Hollow sphere structures for the emission limitation of internal combustion engines"), which was divided into three thematically clearly separated sub-projects.

The intensification of the demands for environmental protection leads to more and more complex exhaust gas treatment systems for internal combustion engines, which will require advanced exhaust gas treatment systems needing increasing installation space and adding weight to the overall treatment system. The increasing complexity of the system increases the flow resistance, which interferes with the charge cycle of the engine. Thus the engine efficiency is reduced and the fuel consumption is higher. Higher fuel consumption increases in general the amount of exhaust gas emitted, which is bad for the environment. Furthermore, particulate filters as well as DeNOx-systems in the exhaust system have to be integrated in a way that the pollutants in the exhaust are reduced to a minimum while the engine performance and the sound emission are not negatively influenced. In principle the exhaust gas systems should be placed close to the engine to maintain the required temperature profile. Since the available installation space (especially close to the engine) is limited in modern cars, the integration of sound insulation and exhaust gas treatment in a combined system seems to be advantageous. The construction of such a combined system is difficult because the functionality of the individual systems have to be guaranteed. Conventional commercial available exhaust gas systems are technically limited according to construction and material properties as well as operating conditions. The overall goal of the project is the development of multifunctional metal hollow sphere structures (HKS) for the simultaneous reduction of sound and exhaust emissions of internal combustion engines for the future abidance of environment protection legislation. A combined system is expected to have competitive advantages compared to conventional exhaust gas systems with modular

concept. The multi-functionality is furthermore related to possible combinations of particulate filter and oxidation catalyst, which is still under development (fig 1).
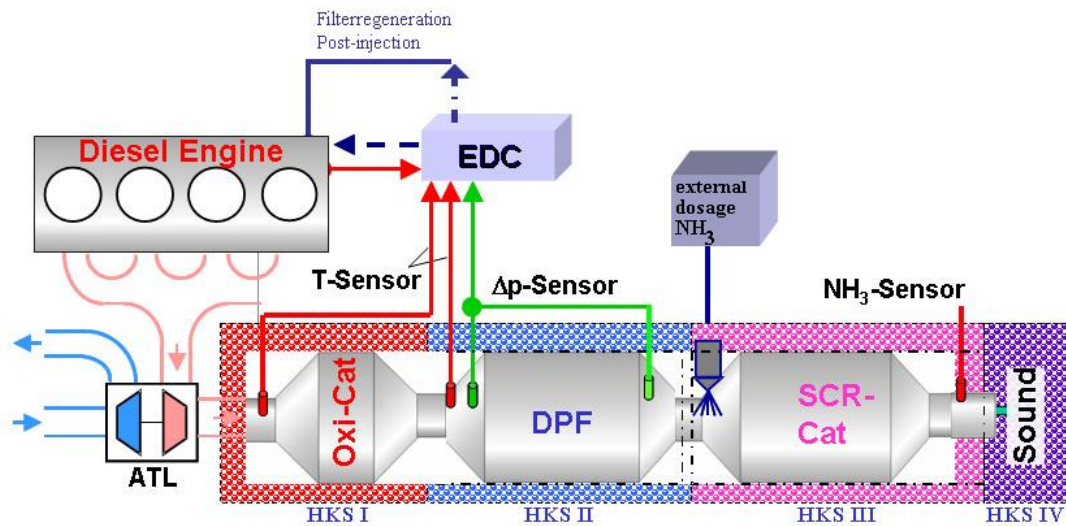
Figure 1: Scheme of exhaust gas system

Exhaust gases from the engine are directed to the exhaust turbo charger (ATL: Abgasturbolader), which improves the efficiency of the engine and then through the oxidation catalyst, the particulate filter, the SCR-catalyst and finally through the sound module. All four parts of the exhaust gas system are potential candidates for the use of a hollow sphere support structure.

2.2 SCIENTIFIC AND TECHNICAL PROJECT GOALS

Despite all efforts for the development of new technologies for mobile applications, the combustion engine will play a major role also in the future. Pollutant emissions, especially particles and nitrogen oxide emissions have to be drastically reduced together with efforts for decreasing fuel consumption. The use of exhaust systems with integrated multipurpose functionalities would help to reduce the weight of the car and therefore have a positive effect on the fuel demand of the engine. A further advantage of an integrated system is the realization of a complex exhaust system consisting of less single parts, which would improve the sound design because each change of diameter influences the overall sound characteristics. Moreover, the conjunction of different modules is always a crucial parameter, so conjunctions should be reduced to a minimum. The overall project goal requires the development of efficient catalyst substrates based on the support made of hollow spheres, which fulfill current requirements of catalysts and which exhibit advantages in regards to noise reduction additionally. Development and research of the integrated exhaust gas system are the main tasks. The use of a high-temperature resisting metal alloy allows the placement of the system close to the engine, which reduces the time until the catalyst reaches the operating temperature and therefore reduced the amount of untreated exhaust gas. The small diameter of the hollow sphere shells is an advantage for the heat conductivity as well.

The development of a catalyst structure based on hollow spheres needs to consider two major areas. First the packing of hollow spheres must allow a certain gas flow that provides high contact time to the surface for a complete conversion of pollutants. Second high temperature and high corrosion resistant material is required to place the structure close to the engine. Furthermore, the noise reducing abilities of the structure should be used and improved. Catalyst and material design have to be combined. The choice of metal alloy for the support structure mainly depends on temperature and corrosion resistance up to 1100°C and thermal shock resistance. The aluminum content in the alloy will be increased to 5 % to

reach the high temperature resistance. The production of hollow sphere structures is based on the coating of a polystyrene substrate with a mixture of metal powder – binder suspension and subsequent sintering. Different types of fine metal powder will be investigated, which differ in morphology, sinter activity and process costs. The metal shell of the hollow spheres is constructed during the coating process out of binder and metal powder. After the production of single spheres, a structure can be made. Further heat treatment sinters the spheres together, while the binder is evaporating. Increasing surface of the support can be achieved with smaller diameters of the spheres, but the flow resistance increases. Research will be focused to find the optimum of surface and flow characteristics in combination with sphere diameter and height of the structure.

After optimization of the structure, the washcoat and the active component have to be stabilized too. The highly porous washcoat increases the surface drastically. Research will be done to apply known concepts for the preparation of traditional ceramic monoliths. The three-dimensional structure of the sintered hollow sphere packing has to be taken into account. The composition of the active component is based on the established Pt system. Optimization and lab-scale production is scheduled. The coating has to be effective for variable pollutant concentrations and mechanical and thermal stress. It will be optimized during all project stages related to activity, stability and shock resistance. The activity of the catalyst is based on an ideal combination of washcoat and distribution of active noble metal. Concepts for combined exhaust gas systems have to be developed besides the research on material and catalytic properties. Hollow sphere structures should be investigated for their applicability in further fields, like SCR-catalyst, too.

2.3 PROJECT ORGANIZATION

The project consortium consisted of seven partners (shown in fig. 2.). The role of TU München was basic research on the development of sintered metal hollow sphere structures for their application as support structure for the emission reduction in exhaust gas systems of internal combustion engines.
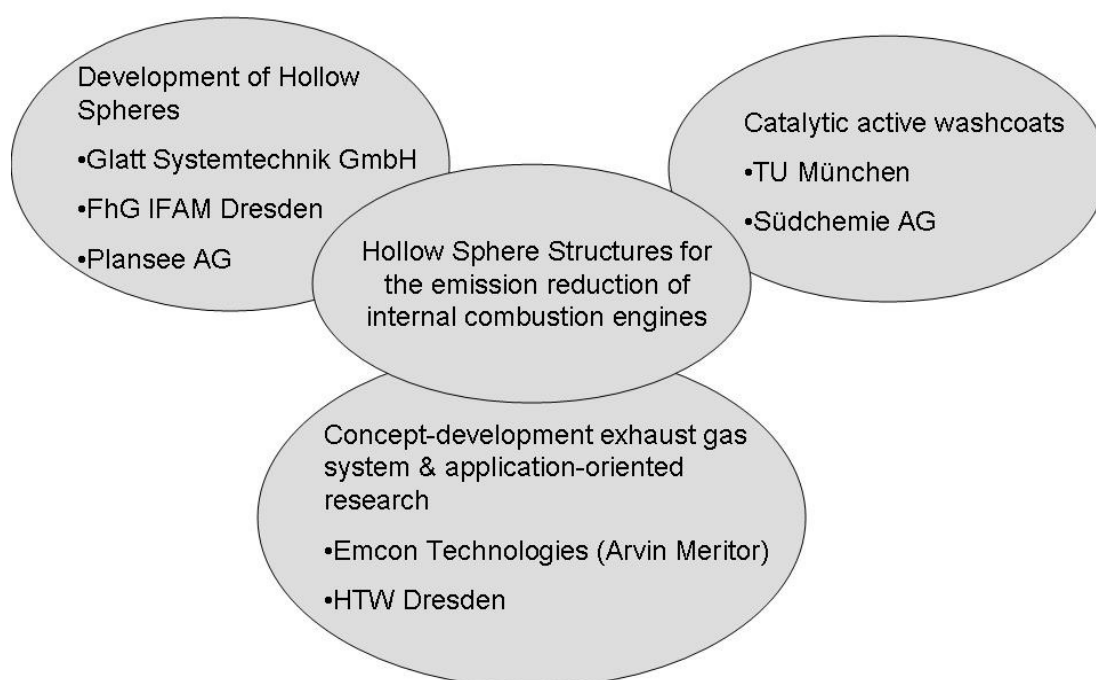
Figure 2: Schematic description of the three combined tasks in the project

The tasks for group 1 (development of hollow spheres) included the selection of materials for the binder, the metal powder and the coating technology, as well as the development of an optimal heat treatment technology and the characterization of sintered hollow sphere structures. Glatt Systemtechnik GmbH, IFAM Dresden located in Dresden and Plansee AG work on the development of hollow spheres. After achieving this step, the production process can be continually improved to cope with desired structure variations and heat treatment technology.

The tasks for group 2 (concept-development exhaust gas system & application oriented research) covered the compilation of technical specifications and the development of a concept for the simultaneous reduction of sound and pollutant emissions of internal combustion engines with sintered metal hollow sphere structures. Emcon Technologies (formerly Arvin Meritor, formerly Zeuna Stärker) located at Augsburg and the Forschungsinstitut Fahrzeugtechnik at Hochschule für Technik und Wirtschaft at Dresden did application oriented research.

Group 3 (catalytic active washcoats) was responsible for investigations on catalytic active coatings, coating technology for sintered metal hollow sphere supports and for the characterization of the catalytic activity for these materials. Südchemie AG and TU Munich, Technical Chemistry II are research partners working on heterogeneous catalysis and reaction technology.

TUM was doing in-situ characterization and tests for the catalytic activity of sintered stainless steel hollow sphere structures as main tasks. A model tubular-flow setup was designed, built and is available for catalytic testing of model catalyst structures. Experiments for the oxidation of NO to NO_2 and CO to CO_2 were carried out to compare the catalytic efficiency in comparison with commercial available monolithic structures. The preparation of model catalysts and optimization of activity and design is also part of the project. Literature and patent analysis for highly dispersed noble metal clusters on metal oxides and the oxidation of the catalyst support was done. Coating of hollow sphere structures for basic research and development of pretreatments were investigated in combination with testing the adhesion strength of different oxide coatings. The coatings were applied on sintered and rolled stainless steel foils in order to find the best support morphology. Catalytic properties are determined with X-ray Diffraction (XRD), Scanning Electron Microscopy (SEM), and X-ray Photoelectron Spectroscopy (XPS). Furthermore neutron tomography and x-ray tomography were used to visualize microscopic and macroscopic hollow sphere structures.

Chapter 3

3 Preparation and characterization of dip-coated materials on sintered Fe-Cr-Ni foils

3.1 ABSTRACT

The effect of sintering of metal surfaces on the adhesion strength of oxidic coatings was investigated. Surfaces of coated foils were characterized using XRD, SEM and the Grid-Cut method according to DIN EN ISO 2409. Sintered Fe-Cr-Ni foils showed generally better adhesion strength than rolled Fe-Cr-Ni foils. A washcoat with desired strength was achieved with 5 % bohemite slurry with a pH of 5. Different oxidic washcoats, different ranges of pH, solid content, as well as growing zeolite β on the surface lead to higher weight loss after testing.

3.2 INTRODUCTION

The preferred material of catalyst support material in applications requiring good heat transfer, complicated flow paths and mechanical robustness are metals, because of their high thermal conductivity and good ductility [1]. One application is the metallic support structure of exhaust catalyst in mobile application such as the diesel oxidation catalysts, where the catalytic function is generated by coating the metal surface with an oxide layer, the so called washcoat, which acts as a reactive interface for depositing small noble metal clusters [2, 3]. Heat-resistant metal alloys, made of Fe-Cr-Ni, are more stable against high temperatures compared to conventional ceramic monoliths [4], therefore, metallic substrates are increasingly used in many fields, especially in automotive exhaust emissions control. Generally, first one or multiple layers of oxides are coated onto the surface of the metallic substrate in order to create a high surface area interface for anchoring the catalytically active (noble) metal particles. If a conventional coating process is used for the coating of the metal support the oxides often peel off easily from the metal surface due to differences in thermal expansion coefficient. Therefore, the adhesion of the washcoat to the metallic substrate has been an important subject for the application of metallic substrates, but

correlations among slurry properties, coating efficiency and washcoat quality are very sparse in the literature. The most important point is the adhesion of the washcoat on the support [5-7].

Sintered stainless steel alloys are a new possibility to enhance the adhesion of the washcoat. In the present work we focus on sintered Fe-Cr-Ni steel metal foils, which were coated with washcoats consisting of bohemite, silica, titania as well as zeolite ß and compare the adhesion behavior with Fe-Cr-Ni foils which are typically used in standard automotive applications. The composition of foils and the applied washcoat was verified X-ray diffraction, the surface of washcoats was examined by scanning electron microscopy. The adhesion behavior was tested with the grid-cutting test according to DIN EN ISO 2409.

3.3 EXPERIMENTAL

3.3.1 Sample Preparation

Sintered and rolled Fe-Cr-Ni alloy foils containing 24-26 wt.% chromium and 19-22 wt.% nickel were selected as metallic substrate used in metallic catalyst supports. Disks with 13 mm diameter were prepared from the foils and degreased in acetone bath under ultrasonic vibration for 15 min, followed by rinsing with de-ionized water.

3.3.2 Coating of Surfaces

The surfaces of sintered and rolled Fe-Cr-Ni foils were coated with single or multiply layers of washcoat by dipping the foils into the slurry [8]. Coating slurries were prepared with different characteristics such as various pH values, solid contents and washcoat compositions (see table 1). The preparation of slurries was controlled by the ratio of solid contents and de-ionized water. The pH value was adjusted with 1.0M nitric acid solution and tested with a pH meter (Schott Instruments Lab 860). The sintered metal foils were immersed into the slurry for 30 s and removed slowly. The samples were first dried in air at room temperature for 30 min followed by drying in an oven at 120 °C for 1 h. The calcination was carried out in a flow of synthetic air (100 ml/min) at 500 °C or 800 °C for 3 hours. The

coating process was repeated until the washcoat loading reached the target level. Loading percentage is calculated by the equation: loading percentage = $((w_C-w)/w)*100\%$, where w_C represents the weight of the coated foil and w represents the uncoated foil.

Table 1: Properties of washcoat compositions

Washcoat	Slurry [wt-%]	Loading [wt-%]
TiO_2	5 %	5 %
Bohemite	5 %	5 %
SiO_2	5 %	5 %
Bohemite pH = 2	10 %	5 %
Bohemite pH = 5	10 %	5 %
Bohemite pH = 7	10 %	5 %
Zeolith β		1day
Zeolith β		3 days
Zeolith β		6 days

SiO_2 (Degussa Ultrasil), TiO_2 (Degussa), Bohemite (Condea Pural), $Al(iso-pro)_3$ (Merck), and TEAOH (Merck) were used for washcoat preparations.

3.3.3 Determination of the washcoat adhesion with the Grid-Cut Method

The Grid-Cut method is described in DIN EN ISO 2409 [9]. As the coatings of all samples were thinner than 60 µm, cuts with a spacing of 1 mm between were made with a scalpel. The weight loss of coatings due to the grid cuts can be calculated according to the following formula:

$$\Delta W_{coating}[\%] = \frac{W_{coating,before} - W_{coating,after}}{W_{coating,before}} \times 100\%$$

with $\Delta W_{coating}$ = Weight loss due to the grid cuts

$W_{coating,before}$ = Weight of coating before the grid cuts

27

$W_{coating,after}$ = Weight of coating after the grid cuts

Adhesion is defined as the molecular attraction between two layers. The coating layer is protecting the metal surface against the influence of the environment.

3.3.4 Scanning Electron Microscopy

The scanning electron microscope (JEOL 5900 LV: 25kV) was used to investigate the surface of different washcoats and supporting materials. Evaluation of washcoat surface can be compared and used together with other techniques for finding the optimal washcoat for the desired application.
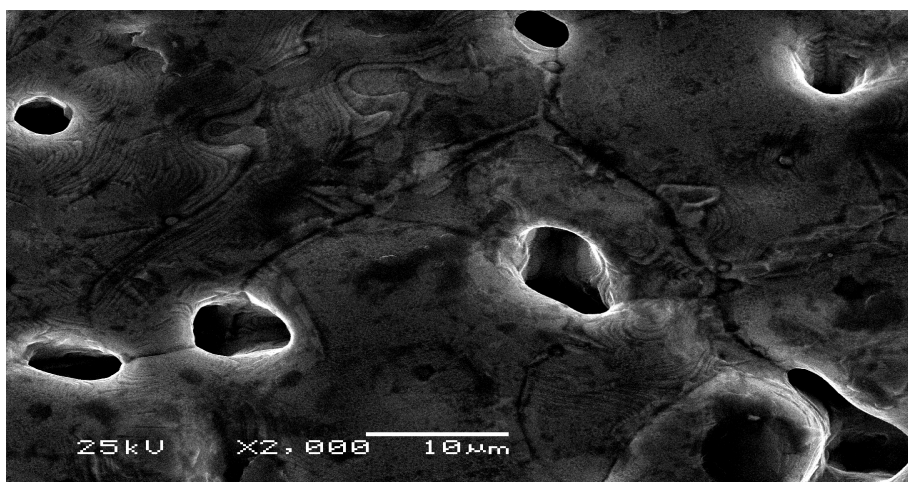
Figure 1: Uncoated Fe-Cr-Ni

Uncoated foil of Fe-Cr-Ni showed holes with a magnification at 10 μm, 5 μm, and 1 μm in figure 1. The SEM pictures of the uncoated foil (thickness 300 μm) reveal holes from the sintering process. These holes with a diameter up to 10 μm are favorable for the adhesion of washcoats on the surface.

3.3.5 X-ray Diffraction

The crystalline structure of the coatings was analyzed by XRD using a *Philips X'Pert Pro System* (CuKα1-radiation, 0.154056 nm) at 45 kV / 40 mA. Phases were identified with the

included database. Measurements were carried out with a step scan of 0.05 °/min from 20°
to 90° (2θ).

3.4 RESULTS

3.4.1 Influence of preparation procedure on surface morphology

XRD measurements were carried out to investigate changes in the structure of bohemite,
and titania during calcination. Silica doesn't change its morphology during calcination.

Bohemite

XRD was recorded for uncalcined and calcined bohemite coating. The changes in the
crystal structure of bohemite powder after the calcination are shown in Fig. 2.
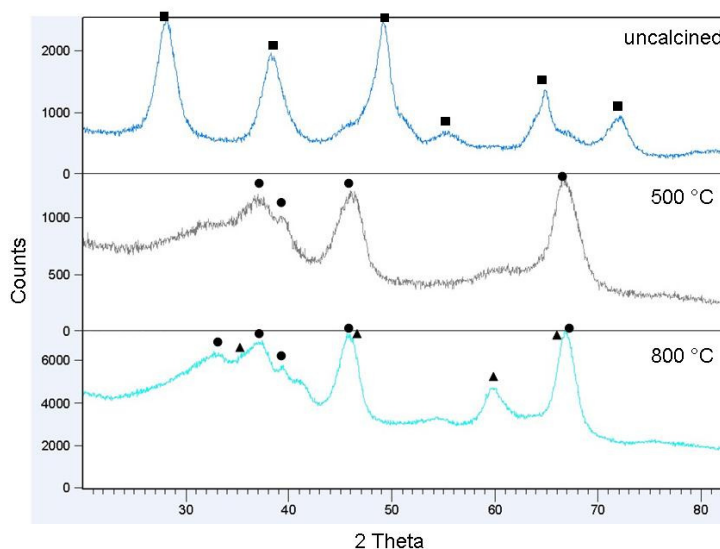
Figure 2: XRD of bohemite before and after calcination at 500 and 800 °C. Phases identified:
■ Bohemite, ● γ-Al_2O_3, ▲ α-Al_2O_3.

The reflexes of calcined bohemite powder show significant differences compared to the
uncalcined sample. The peaks at 28, 38, 49, 55, 65 and 72 °2θ (marked with ■) can be
assigned to bohemite. After calcination at 500 °C peaks typical for γ-Al_2O_3 at 33, 37, 39, 46

and 67 °2θ (●) and after calcination at 800 ℃ also for α-Al$_2$O$_3$ (▲) at 35, 46, 60 und 67 °2θ were observed. At 800 ℃ bohemite was completely transferred to alumina.

Scanning electron microscopy lead to the picture of the surface shown in figure 3.
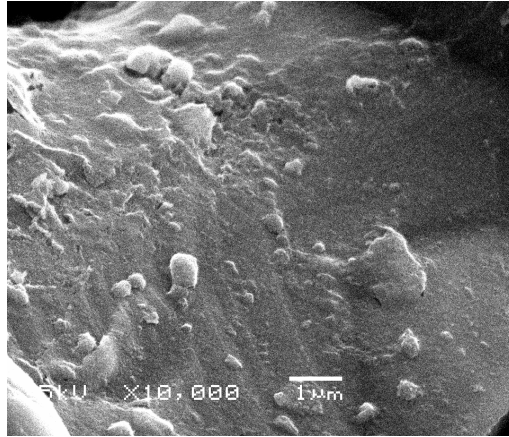
Figure 3: Coated Fe-Cr-Ni

Foil Fe-Cr-Ni was coated with Al$_2$O$_3$ (fig. 3) and recorded with 1 μm.

The surface consists of a layer of calcined bohemite (500 ℃, 5 h). Besides the washcoat layer, the surface exhibits some particles of calcined bohemite too. The particles of alumina are very small. These particles form a very dense, homogeneous layer that covers the surface.

Titania

XRD was recorded for uncalcined and calcined titania coating. The changes in the crystal structure of titania powder after the calcination are shown in Fig. 4.
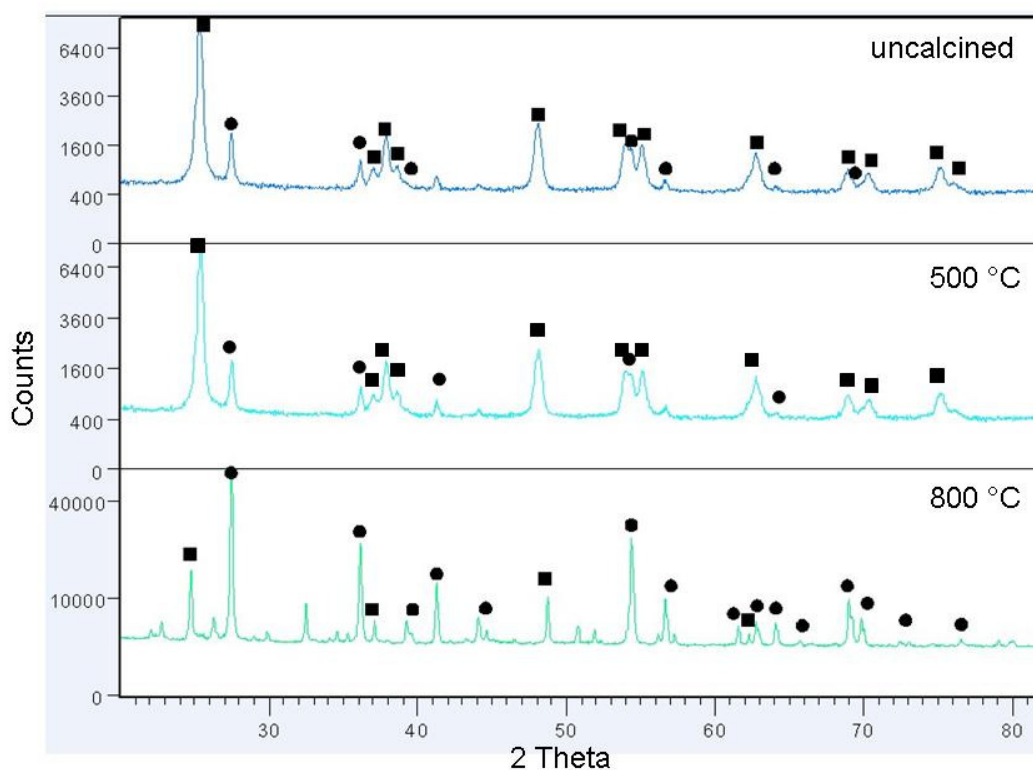
Figure 4**:** Uncalcined TiO_2 and calcined at 500 and 800 °C. ■ Anatas, ● Rutil.

The XRD-peaks of the untreated material are identical to the material calcined at 500 °C. Most reflexes (25, 38, 48, 54, 55, 63, 69, 70 and 75 °2θ) can be assigned to TiO_2 in the Anatas modification marked with (■). After calcination at 800 °C, the structure changed to Rutil (peaks marked with ● at 27, 36, 41, 54, 57 and 69 °2θ) which was already partly visible in the sample calcined at 500 °C, whereas the reflexes from Anatas decreased in intensity. This behavior can be clearly seen in the first two peaks. The most intensive peak

in the first two diffractogramms lost strength in the last one, whereas the signal at 27 ° 2θ

gains intensity after calcinations at 800 °C.

Scanning electron microscopy lead to the picture of the surface shown in figure 5.
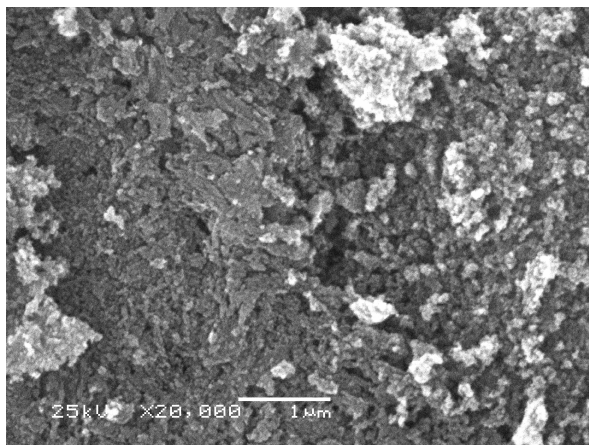
Figure 5: foil Fe-Cr-Ni coated with TiO₂

The coating of Fe-Cr-Ni with TiO$_2$ (fig. 5) lead to a closed washcoat surface with a 1 μm.

Layers of small agglomerates can be seen on the surface. The agglomerates have a less

homogeneous structure than the alumina particles.

Silica

Scanning electron microscopy lead to the picture of the surface shown in figure 3.
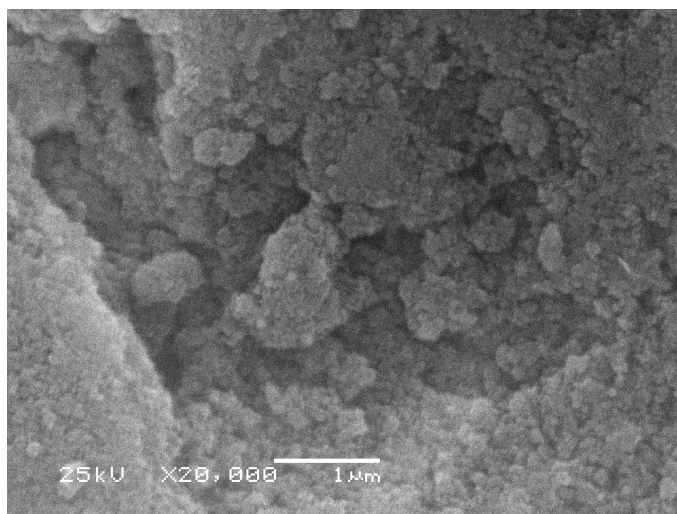
Figure 6: foil Fe-Cr-Ni coated with SiO$_2$

Coating of Fe-Cr-Ni with SiO_2 lead to a closed washcoat surface with 1 µm resolution. Big agglomerates can be determined. They form a layer on the surface that is less uniform than the alumina layer.

3.4.2 Influence of growing time on adhesion properties

Comparison of zeolite ß -washcoats in Figure 7 shows that the zeolite with the longest growing time (6 days) has the lowest weight loss for sintered and rolled foils after applying the grid-cut treatment.
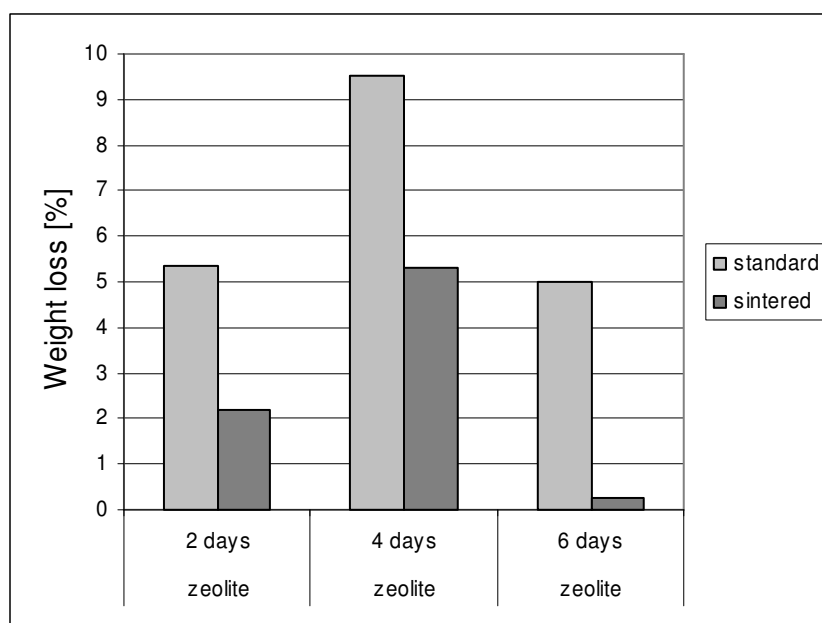
Figure 7: Weight loss [%] of the zeolite coating after 2, 4, and 6 days growing time

The sintered foil with a growing time of 6 days showed a loss of 0.3 % and 5.0 % for the rolled foil. 2.2 % for sintered after 2 days and 5.3 % for sintered after 4 days are significantly lower than 5.3 % for rolled after 2 days and 9.5 % for rolled after 4 days. The norm DIN EN ISO 2409 provides a classification for the adhesion strength on surfaces. The adhesion strength of the rolled foil for the growing of zeolite was determined to 2 for 2,4, and 6 days of growing. In comparison the classification on the sintered foil was 1 for 2 days growing, 2 for

4 days of growing and 1 for 6 days of growing. The following strength of adhesion was observed:

6 days > 2 days > 4 days

Remarkable is that the adhesion of the zeolite growing for six days is better than for 2 days and 4 days. Looking at the zeolite after the preparation procedure reveals solid particles on the surface while a continuous film can be observed on the 6 days growing zeolite. The reason for the better adhesion might be the change of zeolite structure with time during the growing process. The zeolite gel forms bigger particles during the first days of preparation time and then a more homogeneous surface layer with a higher adhesion strength to the surface.
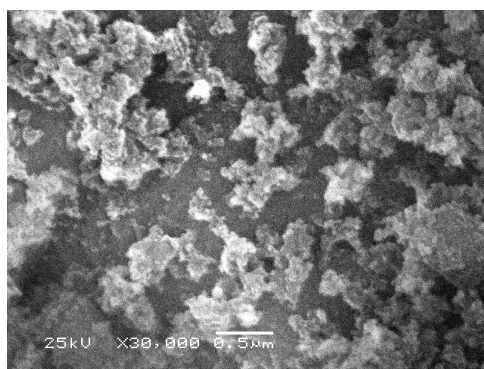
Figure 8: SEM of zeolite growing for 6 days

The SEM picture (fig. 8) displays the zeolite after 6 days. The surface is covered with aggregates of crystallites. The Fe-Cr-Ni was coated with zeolite ß for 6 days. A layer grown on the surface can be seen. The pictures was made with a 0.5 µm resolution on a sintered sample. Zeolite β has a sponge like structure, consisting of agglomerates with ordered crystallites.

Figure 9 compares the XRD patterns of zeolites growing for 1 day and growing for 6 days.
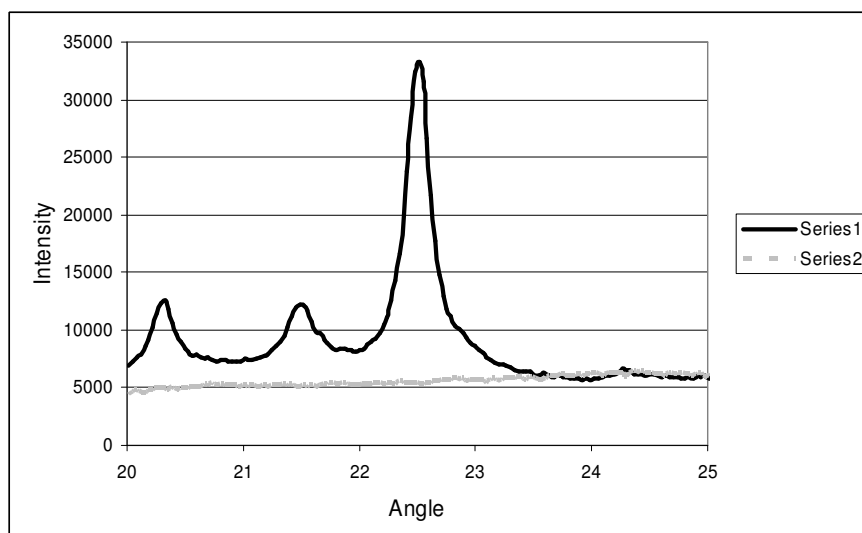
Figure 9: XRD pattern of zeolite: growing for 1 day (grey line), growing for 6 days (black line)

The XRD pattern (grey) after 1 day growing does not reveal the typical zeolite peak, but an amorphous structure, whereas the pattern of the 6 day growing zeolite (black) shows the typical peak at 22 2Theta.

3.4.3 Influence of dip-coated material

Figure 10 compares 4 different washcoats (Bohemite, SiO_2, and TiO2). The highest weight loss was noted for silica with 7.5 % for rolled and 6.3 % for sintered and the smallest for bohemite with 3.6 % for rolled and 2.5 % for sintered. In between was titania (5.0 % rolled and 2.9 % sintered). The order of adhesion strength is:

Bohemite > TiO_2 > SiO_2
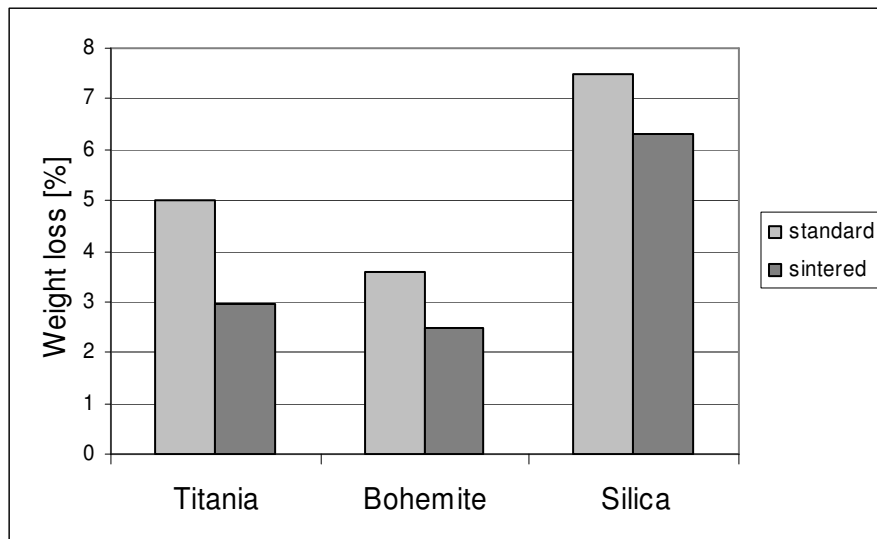
Figure 10: Weight loss [%] of different coatings

The determined classification according to DIN EN ISO 2409 for bohemite was class 1. TiO_2 has class 1 for sintered and class 2 for rolled foils. SiO_2 has class 2 for sintered and rolled foils, as well as Al_2O_3.

3.4.4 Influence of pH on adhesion properties

Interesting for car applications is the bohemite washcoat which was varied regarding pH and composition. Bohemite washcoats show different adhesions depending on the type.
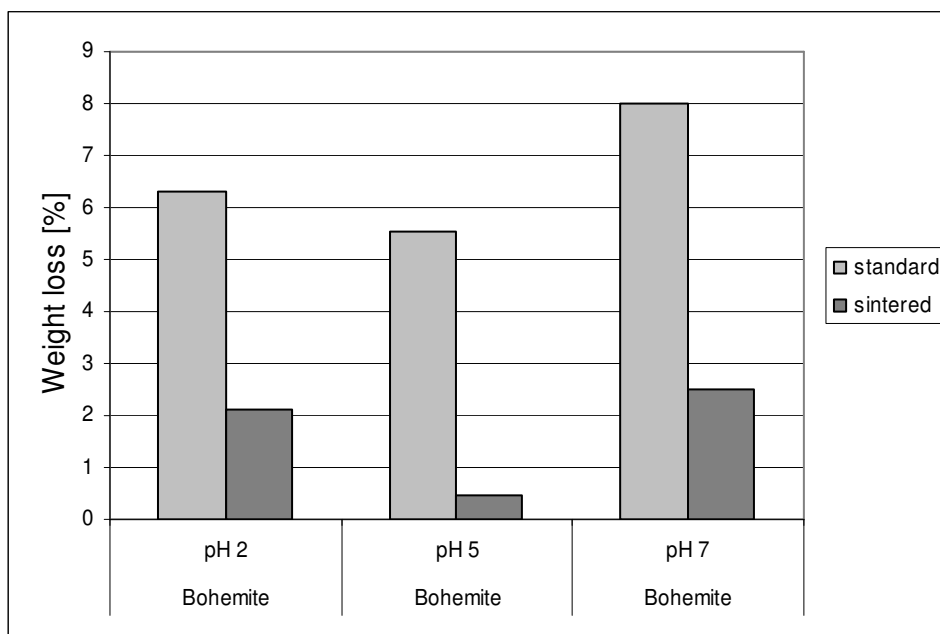
Figure 11: Weight loss of bohemite samples at different pH

The smallest weight loss (fig. 11) is observed for a 10%-slurry-bohemite with pH = 5 (5.6 % for rolled and 0.5 % for sintered). 10%-bohemite with pH=2 has a higher weight loss with 6.3 % and 2.1 %. 10%-bohemite with pH=7 has the highest weight loss with 8.0 % and 2.5 %. The order of adhesion strength was as followed:

pH = 5 > pH=2 > pH =7

Rolled foils were determined to type 2 for all washcoats while sintered foils were type 1.

3.5 DISCUSSION

The preparation procedure to apply coatings to metal surfaces influenced the morphology. After calcination at 800 °C the dip-coated bohemite was transferred to alumina and the titania modification changed from anatas to rutil, shown by XRD, while the surface of dip-coated silica did not change. Further characterization of the surface with scanning electron microscopy revealed a smooth surface for bohemite samples with very small particles forming the coating layer. In contrary, silica exhibits much bigger round-shaped agglomerates on the non-uniform distributed layer, as well as the inhomogeneous distributed jagged-shaped agglomerates of titania. The Fe-Cr-Ni foils, sintered and rolled, showed different behavior in their adhesion strength of the coatings. The adhesion test gave the following sequence: Bohemite > titania > silica. The highest weight loss was noted for silica with 7.5 % for rolled and 6.3 % for sintered and the smallest for bohemite with 3.6 % for rolled and 2.5 % for sintered. The determined classification according to DIN EN ISO 2409 for bohemite was class 1. SiO_2 has class 2 for sintered and rolled foils, while titania showed results in between. The weight loss of rolled foils is always higher compared to sintered foils for all investigated samples. The low weight loss of the bohemite coating was further investigated with changing the pH of the slurry for the dip-coating procedure. The smallest weight loss is observed with pH = 5 (5.6 % for rolled and 0.5 % for sintered). Bohemite slurry with pH=2 has a higher weight loss, as well as the slurry with pH=7. The determined classification according to DIN EN ISO 2409 was 2 for rolled foils while sintered foils were type 1 at each pH value.

Zeolite β was coated on sintered and rolled surfaces because zeolite forms very small nanoparticles, which could follow the trend to improve the adhesion strength. The sintered foil with a growing time of 6 days showed a loss of 0.3 % (norm type 1) for sintered and 5.0 % (norm type 2) for the rolled foil. After 2 and 4 days the weight loss was higher. The XRD pattern of the growing zeolite after 1 day does not reveal the typical zeolite peak, but an amorphous structure, whereas the pattern of the 6 day growing zeolite shows the typical peak at 22 °2θ. However, SEM shows a non-uniform layer on the surface and the

preparation time of six days is too long for an efficient industrial coating process. The field of application for the investigated foils is as support for car catalysts. Fe-Cr-Ni alloys in different shapes, monoliths or hollow spheres, are coated and impregnated with the active metal Pt for diesel oxidation catalysts.

The principle behind good adhesion strength is the interconnection between metal surface and coating layer. A small particle size forms a dense and stable layer shown by the bohemite slurry with pH 5. During the calcination process, bohemite can bind better to the surface, which results in a lower weight loss.

During the sintering process, small particles are combined to bigger structures, which form the sintered foil. The arrangement of the particles is not perfect during this process. An almost regular surface with defects (holes with diameters between 5-10 µm) can be observed. In comparison with rolled foils, these sintered samples have a much rougher surface, which explains the lower weight loss (all investigated coatings) due to a higher contact area. The defects in the structure increase the available surface for the binding coating compared to the flat areas on rolled foils.

3.6 CONCLUSION

Important for adhesion of coatings on metal foil is the preparation method, depending on pH, concentration, calcination temperature, and chemical composition. All these factors influence the interconnection between Fe-Cr-Ni surface and coating. The surface morphology of sintered samples showed a rougher surface than rolled foils which creates more surface. Better adhesion was achieved for all tested washcoats on sintered support. A pH of 5 for a slurry of bohemite lead to the best adhesion performance. The weight loss measured according to DIN EN ISO 2409 induced by the grid-cut method could be controlled below 1% for sintered foils. The significant advantage of the bohemite, calcined coating exhibits small particles, was shown with SEM. Furthermore, XRD and adhesion test were used to show the advantage over silica, titania and zeolite β.

3.8 REFERENCES

[1] J.P. Reymond, Catalysis Today 69 (2001) 343

[2] P. Forzatti, Catalysis Today 69 (2001) 307

[3] J.F. Watton, US 4279782 (1981)

[4] A.M. Hilmen, Catalysis Today 69 (2001) 227

[5] J. Wang, Surface and Coatings Technology 201 (2007) 7159

[6] X. Wu, Surface and Coatings Technology, 190 (2005), 2-3, 434

[7] S. Zhao, Surface and Coatings Technology, 167 (2003), 97

[8] E. Tronconi, Applied Catalysis B: Environmental, 62 (2006), 121

[9] DIN EN ISO 2409

Chapter 4

4   Understanding of hollow sphere structures for emission control catalysts

4.1 ABSTRACT

Stainless steel hollow sphere structures used as support for catalytic active coatings in automotive emission reduction are promising new materials for catalyst systems because of their ability to be applied in multipurpose applications. The quality of the manufacturing process, which influences the pressure drop over the catalyst and consequently the catalytic activity, is a crucial parameter. This study will introduce neutron imaging as a tool for the non destructive inspection of the macroscopic structure of hollow sphere catalyst support structures. The geometric properties of the support structures will be related to the pressure drop and catalytic properties, and the suitability of hollow sphere structures as supports for car exhaust catalysts will be discussed.

4.2 INTRODUCTION

In modern car exhaust gas treatment the commonly used oxidation catalysts are based on monolithic supports with mostly straight pores. Besides the traditional ceramic support material cordierite, metal structures are increasingly used due to a longer lifetime, a lower heat capacity and an enhanced mass transfer resulting from introducing tortuosity into the pores by using corrugated walls. To reach the limits for NO_x, CO and hydrocarbon emissions specified by legislation catalysts will be necessary for cars with Diesel as well as with Otto engines. The upcoming stringent emission legislations in Europe (Euro 5, Euro 6) and the US (US 07) require a constant improvement of the catalysts with respect to the active materials as well as the support structures.[1-3] In ceramic as well as metallic honeycomb structures the exhaust gas flows through the coated channels and reacts on the precious metal particles deposited on the

channel walls. In the typical monolith structure with flat walls the gas reaches rapidly a laminar flow pattern after entering into the channels, which leads to severe mass transfer limitations. As potential solutions metal monolith structures with corrugated walls were introduced, which generate turbulences inside the channels after the ramps and holes imprinted into the walls[4]. The enhanced radial mixing of the gas is, however, invariably coupled to an increased pressure drop.

A new approach is the use of metallic hollow sphere structures as catalyst support, which are produced in a sintering process.[5] Variations in the diameter and material of the metal spheres as well as in the geometry of the sintered structure allow a flexible adaptation of the carrier to the specific demands of the particular catalytic application. A multifunctional combination between catalytic properties, particle removal and sound insulation appears to be feasible with these hollow sphere structures. The key feature for those applications is the diameter and the packing of the individual spheres to the macroscopic support structure. Catalytic applications such as (hydrocarbon and NO) oxidation require in general small diameters of the spheres in order to maximize the geometrical surface for anchoring the catalytic active species, while for acoustic applications (i.e., sound insulation) parameters such as tortuosity and porosity play the key role[6]. Besides these principle design parameters the dense packing of the spheres influences the pressure drop, which should be in general low, and possible bypassing of the catalysts by channeling effects, which leads to lower conversion and, therefore, has to be avoided. To fulfill all requirements for the three fields of potential application, detailed information on the macroscopic arrangement of the hollow spheres in the three-dimensional structure is essential.

Neutron-tomography, a new non-destructive technique was used to study the ordering of the individual hollow spheres inside the structure. From the results of the neutron tomography the free volume between the spheres was calculated and compared for structures produced in different series in order to explain the influence of the packing of the spheres on the catalytic

properties and the pressure drop. The advantage of neutron tomography is that it allows the generation of three-dimensional images of the carrier structure and, because it is a non-destructive technique, the same sample can be investigated before, during and after testing in an engine test bench. In conventional neutron radiography, the absorption contrast is calculated from the attenuation of the neutron beam passing through the object, which varies as a function of the density of the material or at the interfaces between different materials. In neutron tomography, several radiographies of an object are collected under different angles of the sample with respect to the neutron beam and from this set of projections a three-dimensional model is reconstructed. In this model slices through the inner structure can be visualized and analyzed. Besides this conventional technique for non-destructive testing, which was already used by Röntgen (investigations with x-rays), the wave characteristics of the neutron can be utilized to obtain additional information from the phase contrast. On its way through the object, the neutron beam is not only attenuated, its phase is also shifted. If the neutron beam has a high transversal spatial coherence and the detector is in a suitable distance from the object (in the near filed region), interference effects can be utilized to enhance the contrast at edges and interfaces of an object[7]

This work focuses on the non-destructive investigation of hollow sphere assemblies used as advanced support structures for car exhaust catalysts. Neutron absorption imaging and phase contrast imaging using cold neutrons were compared and used to explain the differences of hollow sphere support materials with regard to channeling, its influence on the pressure drop, and the catalytic activity.

4.3 EXPERIMENTAL

4.3.1 Materials

The materials were prepared by IFAM (Dresden), Glatt Systemtechnik GmbH and PLANSEE. For producing the hollow sphere structures polystyrol spheres were coated with a nanoparticle sized stainless steel alloy. A three-dimensional structure was formed from the spheres and during the subsequent sintering the polystyrol was removed and the metal particles form a dense shell constituting a hollow sphere.[5, 8, 9] Two stainless steel materials (1.4841 and 1.4767, in the following called catalyst A and catalyst B) were used for the hollow sphere support structures. Material compositions are given in Table 1.

Table 1: Material compositions [10]

	Cr	Ni	Mn	Si	C	S	P	Al	O	Fe
catalyst A	24-26	19-22	<2	1,5-2,5	<0,2	0,03	0,045		<0,1	balance
catalyst B	19-22		<1	<1	<0,1	0,03	0,045	5		balance

Two structures produced from spheres with a diameter of 3 mm and two structures from spheres with a diameter of 6 mm were investigated. The structures were coated with a standard washcoat based on Al_2O_3 and impregnated with Pt (100 g/ft³) a formulation typically used for oxidation catalysts.[11, 12]

Figure 1: Images of small model structures and the macroscopic structure used in an engine test bench

Figure 1 shows the (small) hollow sphere structure formed from spheres with 3 mm diameter at the left and the (large) hollow sphere structures formed from spheres with a diameters of 6 mm at the right. After investigating the small hollow sphere structures with neutron tomography, its catalytic activity for the oxidation of NO and the pressure drop was investigated. The large structure was used in a diesel engine test bench at the facilities of a project partner (WING initiative: project number 03X3004) and tested for visualization of defects in the macroscopic structure.

4.3.2 Neutron Tomography

The experiments were performed at the radiography facility ANTARES at FRM-II (Munich). A schematic layout of the experimental layout is shown in figure 2.[13]
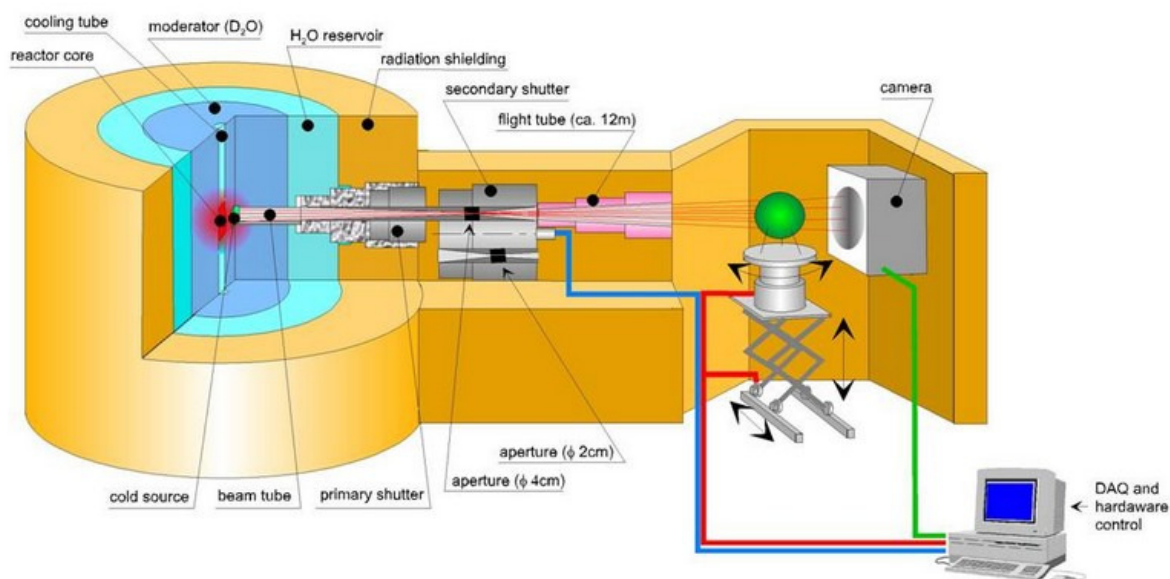
Figure 2: Schematic layout of the experimental facility ANTARES at FRM-II

The facility is located at a cold neutron beam at FRM-II. A multifilter was installed, which allows the utilization of different crystal filters to reduce gamma radiation and epithermal neutrons (neutrons of kinetic energy greater than that of thermal agitation)[14] or to modify the neutron spectrum. The sample is placed on a rotary table, which is mounted on a manipulator to position the sample in the neutron beam. A LiF-scintillator converts neutrons into visible light, which is detected by a CCD camera with 2048 x 2048 pixels. The maximum sample size of the ANTARES station is 30 cm, which allows investigating the catalyst carriers directly. During a routine tomography, the sample is rotated in 200 to 800 angular steps from 0° to 180°. The neutron-flux intensity is 10^8 (cm^{-2} s^{-1}) for L/D=400, with L the distance between aperture and sample and D the diameter of the aperture.

In conventional neutron radiography, the image results from the attenuation of the neutron beam during its propagation through the object investigated. In phase contrast neutron imaging, the wave characteristics of the neutrons are utilized to enhance the contrast. For phase contrast studies, a pinhole aperture is introduced into the neutron beam (the L/D ratio can be varied from 400 to 14000), and the sample-detector-distance has to be increased to obtain interference effects[15] .

Table 2: Parameters for ANTARES

Imaging technique	Conventional method I	Conventional method II	Phase contrast
L/D ratio	800	800	7000
Sample-detector distance	8 cm	8 cm	130 cm
Pixel size	100 μm	50 μm	100 μm
Exposure time	7 s	30 s	20 min

In general the quality of the results of neutron tomography (NT) is mainly influenced by the quality of the single radiography projection images. The best results are achieved in an almost parallel neutron beam, characterized by a high collision ratio L/D [16]. However, the smaller the distance to the scintillator plane and the object size, the lower the geometrical distortion of points in the projection image. Collision ratios of several hundreds are provided by neutron flight tubes.

The images were reconstructed from the projections on the CCD chips (2048 x 2048 pixels) using open beam and dark current images to normalize the data set. Details of the reconstruction algorithms and the experimental details are described at Mühlbauer et al.[17]

Different colors were assigned to specific attenuation coefficients of the materials. The darker areas correspond to a larger attenuation of the neutron beam.

4.3.3 Pressure drop experiments

The pressure drop was measured in a flow reactor from quartz (21 mm inner diameter) using two manometers (Hensel, working range: 0-3 bar, accuracy: 1 mbar) placed directly before and after the reactor (see Fig 3). The hollow sphere structures ($\varnothing$=21 mm, length = 25 – 28 mm, sphere diameters = 3 mm) were packed into the tube using an isolation mat (alumino silicate) and centered in the quartz tube. To increase the accuracy of the experiments five structures were placed into the tube, because the pressure drop of a single structure was too close to the detection limit. The pressure drop was measured at a volumetric flow of 3000 ml/min (space velocity 52000 h^{-1}) at room temperature and 330 °C.

Figure 3: Scheme of the pressure drop measurement system

The pressure drop is linearly correlated with the catalyst length as described by the Hagen-Poiseuille law:

$$\Delta p = \frac{8 \cdot \dot{V} \cdot \eta \cdot l}{\pi \cdot r^4}$$

where $\dot{V}$ is the volumetric flow, η the viscosity, l the length of the catalyst and r the radius of the tube. Note that the structure of catalyst A is about 10% longer than the structure of catalyst B.

4.3.4 Catalytic test reaction

The oxidation of NO with O_2 was studied in a flow reactor and the concentration of products was analyzed with a mass spectrometer with a chemical ionization system (CIMS V&F AIRSENSE 2000).

The reactions were carried out using a gas stream consisting of 4000 ml/min N_2 (carrier gas), 50 ml/min O_2 and 4 ml/min NO, which corresponds to a NO concentration of 1000 ppm. The space velocity over the catalyst structure was 70000 h^{-1} assuming a free volume of the hollow sphere structure of 40 %. During the experiments the temperature was increased from room temperature to 500 °C using an increment of 1°C/min while continuously monitoring the concentration of products and reactants.

4.4 RESULTS

4.4.1 Comparison of absorption contrast and phase contrast imaging

Phase contrast imaging was considered so far as the imaging technique with the highest contrast, however, it was not applicable for very long measurement times, e.g., up to three days for this size of object, mainly because stable conditions of the neutron beam could not be maintained over this time period. However, the improvement of the experimental design of the ANATRES station at the FRM-II [15] allows the combination of high resolution and acceptable measurement time. Radiographies of the catalyst structure with 3 mm hollow spheres measured with absorption imaging and phase contrast imaging were compared and differences in the resolution and the contrast can be clearly seen. Table 2 describes the parameters used for the measurements.

The enhanced resolution and contrast of the phase contrast imaging becomes even more evident from the comparison of slices in axial direction after reconstructing the structures for conventional imaging (Fig. 4. left and middle)
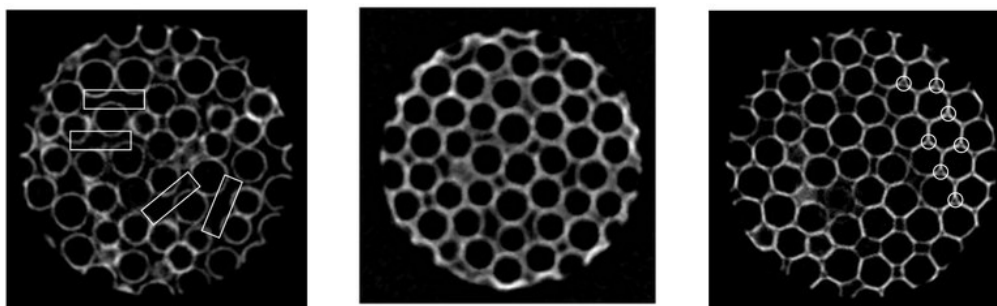
Figure 4: Slices of reconstructed tomographic images: catalyst A conventional imaging method I (left), catalyst A phase contrast imaging (middle), catalyst B conventional imaging method II (right)

Both pictures represent the same slice through the structure. Better quality was achieved in the case of phase contrast imaging using with higher L/D ratio and exposure time. Due to the long time required for this measurement mode of about 3 days for one experiment, this technique is possible but not yet feasible for standard experiments. The contours of the hollow spheres are principally already visible with the conventional imaging method, but the phase contrast imaging method allows a much clearer visualization of the macroscopic inner structure with less smearing inside each hollow sphere. All areas without material should be black, which is clearly achieved with the phase contrast imaging, while for conventional imaging, there are different grey-scale impurities visible as artifacts inside the hollow spheres. To study the homogeneity of the arrangement of the spheres in the model structure, an axial slice through the structure was calculated and is shown in Figure 4. The white squares indicate zones in the structure where the neighboring hollow spheres do not touch each other and lead to open channels inside the structure. These defects were frequently observed in the structure of catalyst A (Fig 4 left), while tomography indicates a much better packing for the structure of catalyst B. The white circles show areas were neighboring hollow spheres touch each other in the most densely way. There are almost no spaces between hollow spheres, leading to a homogeneous packed structure.

In three dimensions the regular arrangement of equal sized spheres leads to different packaging densities. The body centered cubic (BCC) structure contains eight spheres on each corner of the cube and one in the center. The atomic packing factor, or packing fraction, is 0.68. The face centered cubic (FCC), also called cubic closest packing (ccp) and the hexagonal cubic packaging (HCP) have both a packing factor of 0.74. All structures are produced as a uniform, global irregular, structure with an average packing fraction of 0.60 (supplied by producer).

4.4.2 Tomography on structures with 3 mm sphere diameter

Radiographic images were recorded for the hollow sphere structures with 3 mm sphere diameter of catalyst A and B, the axial view of the calculated 3D model is shown in Fig. 5. Contours of the hollow spheres can be clearly seen and the images indicate that not all spheres are densely packed. The open areas between the spheres presumably present interrelated cavities and channels. Moreover, several deformed contours are detected. To determine the free volume of the hollow sphere structures of catalyst A and B the open spheres in a frontal cut of the two 3D reconstructed models in a given area (20 x 20 mm) were counted (marked with circles in Fig. 5).
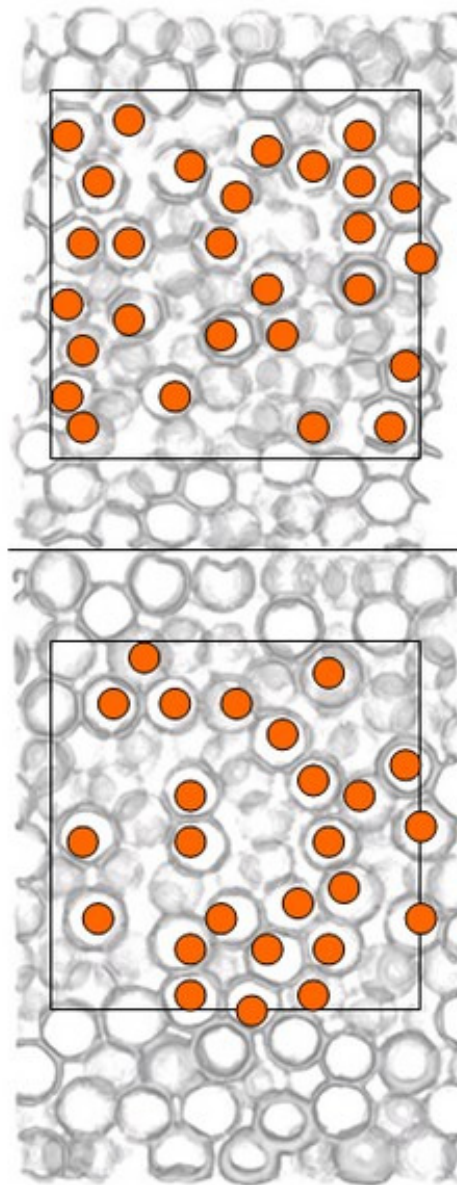
Figure 5: Frontal cut of two hollow sphere structures (catalyst B above catalyst A), recorded with method II

The square area in the slice through catalyst B (fig 5 top) contains 28 open spheres. For catalyst A (fig 5 bottom) 24 open spheres were detected through the structure. Using the size of the structure and an average sphere diameter of 3 mm the open area for catalyst B (Fig. 5 top)

was 57 % and for catalyst A (Fig. 5 bottom) 63 %. Uncounted incomplete spheres reveal a disadvantage of this method, leading to higher open areas.

4.4.3 Catalytic activity

The conversion of NO over the catalysts using supports from catalyst A and B at constant volumetric flows (4ml NO, 50ml O_2, 4000ml N_2) in the temperature range between 50 and 500 °C is compared in Fig 6. The general trend for both supports shows an increasing conversion up to the maximum at ~330°. At higher temperatures the concentration of NO_2 starts to decrease as the concentration reaches the limit given by thermodynamic equilibrium between $NO+O_2 <-> NO_2$. With increasing temperature the equilibrium constant (i.e. $K = [NO_2]/([NO]\cdot[O_2])$ decreases and consequently the conversion of NO decreases. Only catalyst B reached the equilibrium level of NO_2, while catalyst A showed a maximum conversion significantly below the equilibrium level of NO_2.
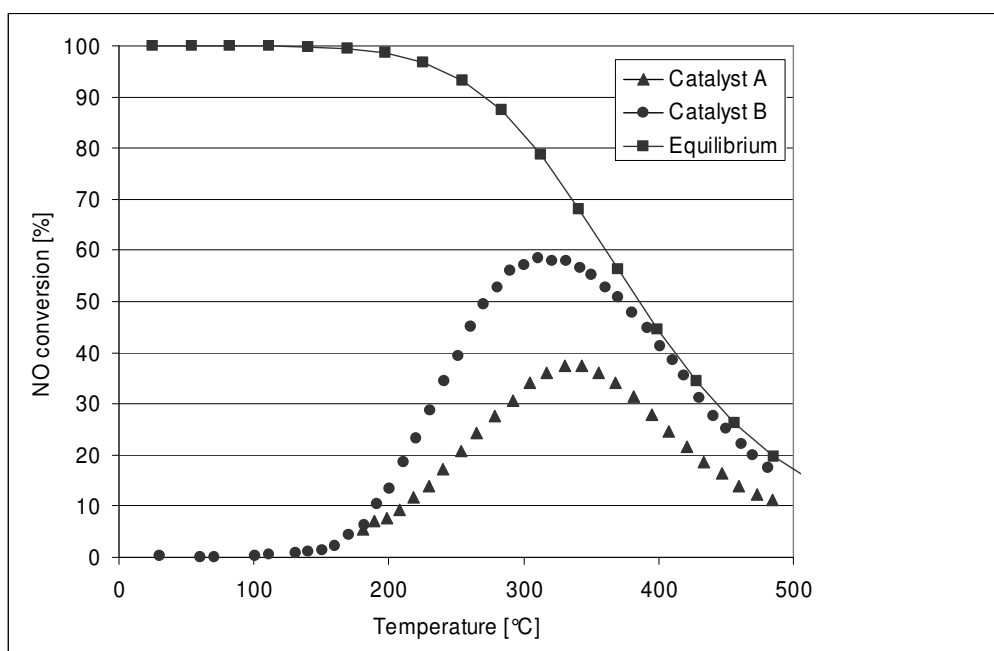
Figure 6: NO conversion over temperature for model catalyst structures; dots: catalyst B, triangles: catalyst A, squares: equilibrium

4.4.4 Pressure drop

The pressure drop at room temperature and at 330 °C over the catalysts A and B are compared with a traditional monolith (cordierite 400 cpsi) in figure 7 (five structures were inserted). The pressure drop was measured with uncoated model catalysts. At room temperature the pressure drop was 0.5 and 0.6 mbar for catalyst A and B structures, respectively, and increased at elevated temperatures (330 °C) to 1,65 and 2,6 mbar. In contrast pressure drop for the monolithic structure was barely detectable (0.1 mbar) in comparison with hollow sphere structures.
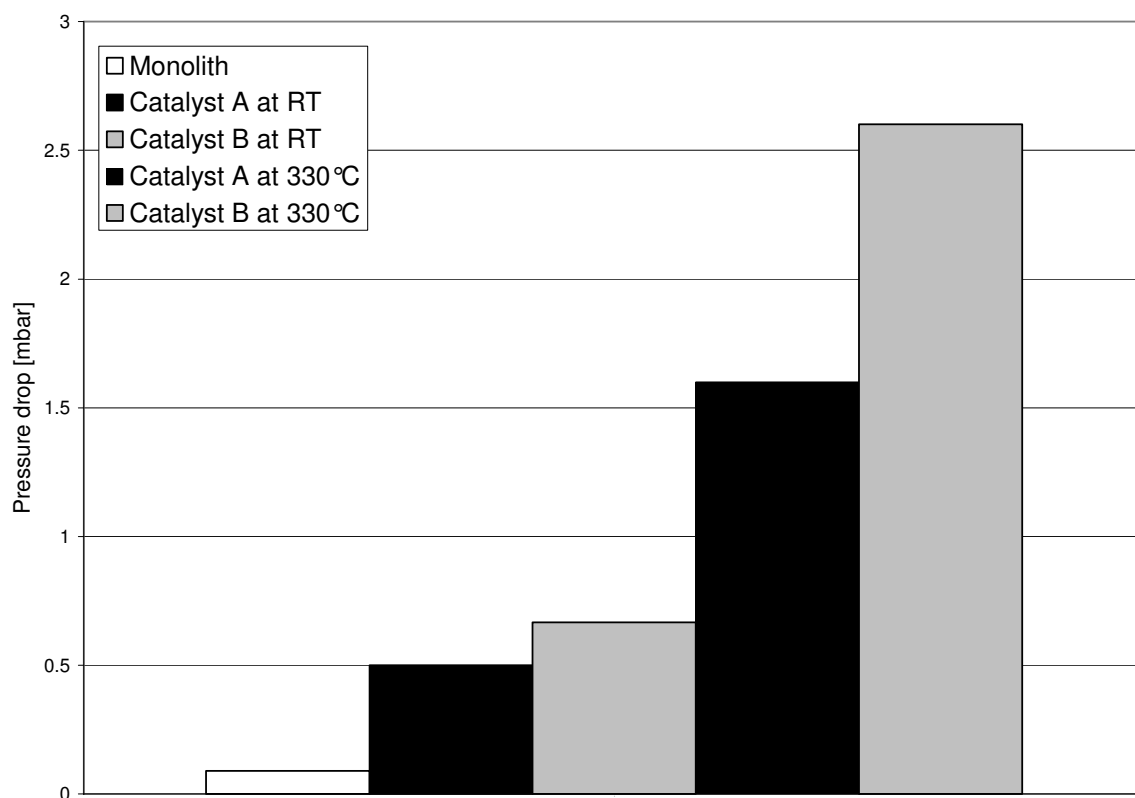
Figure 7: Pressure drop at room temperature and elevated temperature for monolith, catalyst A and B

It has to be noted that the structure with the higher pressure drop (catalyst B) was slightly shorter i.e. 25 mm compared to the catalyst A structure i.e. 28 mm. As the pressure drop is linearly dependent on length the differences between the two materials will be even more pronounced on structures with the same length. Monolithic catalytic systems in cars have a total pressure drop around 100 mbar depending on open frontal area, catalyst length and cell density.[18-20]

4.4.5 Hollow sphere structure with 6 mm sphere diameter

Radiography measurements of the hollow sphere structure consisting of spheres with 6 mm diameters were carried out under the same conditions as described above for absorption imaging. The 3-dimensional view of the structure is shown in Fig. 8. The resolution of the detector (100μm) allows a magnification with a factor of 4 (shown in figure 8 right side) which gives a detailed view of the hollow spheres and their surface structure.
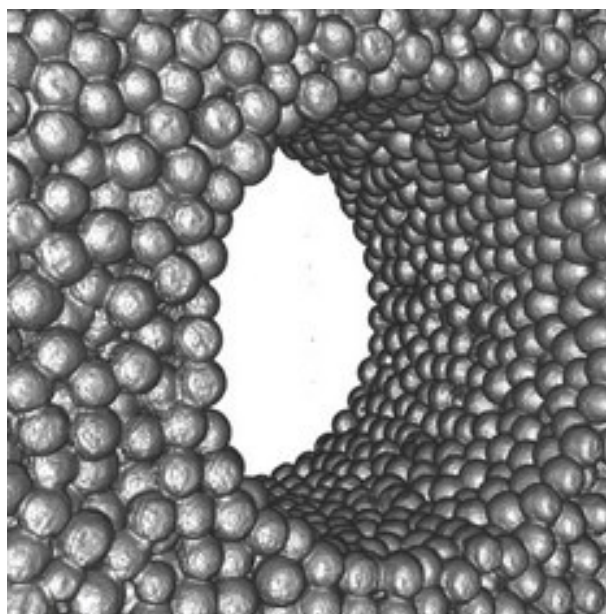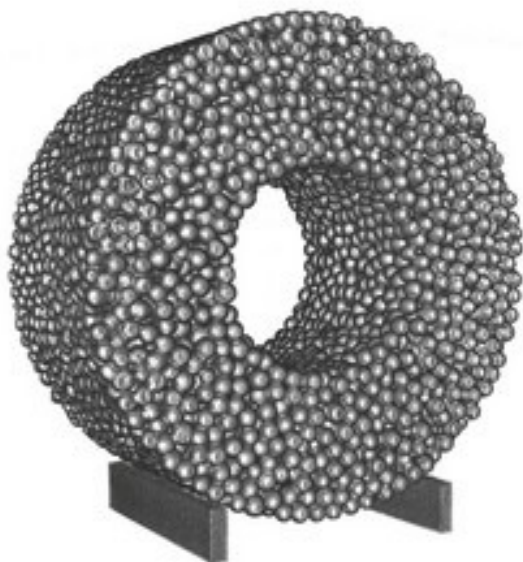
Figure 8: 3D images of the macroscopic structure

Two reconstructed axial slices (tomographies) through the structure are shown in Fig.9. The left image gives a general overview of the 3D structure of the hollow spheres inside the macroscopic support structure. In the image on the right side two square areas are marked, on the left side and on the bottom. In those marked areas the hollow spheres were counted and the free area was determined to be 45 % in both cases.
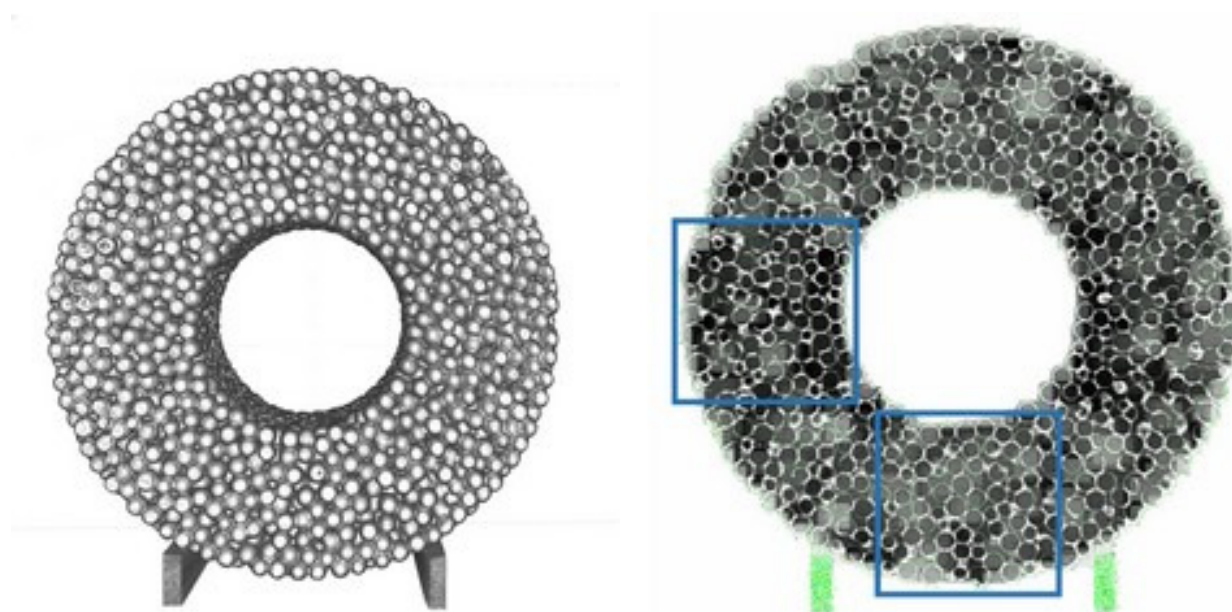
Figure 9: Cut through axial direction; recorded with method I

4.5 DISCUSSION

Neutron tomography is a powerful tool for the non-destructive analysis of catalyst support structures for automotive applications and the improvement of the contrast by phase contrast imaging was clearly observed. For the structures consisting of hollow spheres with 3 mm diameter the density of the packing was evaluated form the fraction of spheres in the plane of the axial cut of three-dimensionally reconstructed structures. Depending on the preparation of the hollow sphere support differences in the packing density and the interconnection of the individual spheres were observed, leading to open channels thorough the catalysts support structure. A calculation of the free area in randomly selected areas resulted in a free area of 57

% for catalyst B and 63 % for catalyst A. On both structures the NO conversion showed a maximum at around 330 °C. The maximum conversion of NO was about 40 % for catalyst A and about 60 % for catalyst B. The difference in conversion results from the lower available Pt surface in catalyst A due to several reasons. Because of the lower packing density in the structure of catalyst A, less hollow spheres and, therefore, less active Pt surface was provided for the reaction as well as channeling effects are more likely to occur influencing the uniform distribution of the gas inside the structure. Although the presence of channels reduces the pressure drop over the structure, the lower residence time for the reactant molecules inside the catalyst leads to a lower conversion as shown for catalyst A compared to catalyst B. If the reactant flow is not distributed in a uniform way throughout the structure, negative effects regarding catalytic function occur. At high temperature the NO conversion reaches the thermodynamic value over the dense packed structure, which indicates that inside this material the residence time is uniform and the turbulent flow of the gas between the spheres lead to an efficient mass transfer. In contrast for the more open structure a fraction of the gas passes through the channels between the spheres without contact to the catalytic sites and therefore the conversion is lower (channeling effects).

The comparison of the structural properties, the pressure drop and the catalytic activity clearly showed that the general advantage of the hollow sphere structure, i.e. the enhanced mass transfer resulting from the turbulent flow inside the structure, can only be realized if the individual single spheres are densely packed and in close contact. Although this leads to an enhanced pressure drop compared with typical monolith structures, some application might benefit from the higher conversion levels. This example illustrates the necessity of techniques for non destructive analysis of the hollow sphere structures: Only a dense packing and the absence of open channels through the structure allows the utilization of the advanced properties of these supports. Otherwise the disadvantage of the high pressure drop will not be compensated by an enhanced conversion over the catalyst.

For the structure with 6 mm spheres differences in the contact between the spheres and the shape of the single spheres resulting from the production process were observed. The packing density, however, was the same (45 % free volume) throughout the structure.

4.6 CONCLUSIONS

The non-destructive investigation of stainless steel hollow sphere structures by neutron tomography is an important method for the characterization of the quality and the manufacturing process of these catalyst support structures. Phase contrast imaging increased the resolution of the images, thus allowing a detailed investigation of the geometrical properties for the single spheres. The hollow sphere structures led to an enhanced catalytic activity in the NO oxidation, which can only be utilized over densely packed structures. In the presence of open channels the activity is decreased and the generally higher pressure drop over these materials will not be compensated by the enhanced mass transfer. Thus advanced characterization methods, such as tomography, will be essential for the development and the utilization of these novel catalyst support structures.

4.7 ACKNOWLEDGEMENT

4.8 REFERENCES

[1]   E. S. Joubert, T.; Weinstein, N., in *Diesel Engine Emission Reduction Conference (DEER)*, Coronado, California, 2004.

[2]   http://www.dieselnet.com/standards/, 2007.

[3]   T. Johnson, *SAE International* 2004, *2001-01-0070*.

[4]   E. Jobson, M. J. A., A. Cauvel, F. Jayat*, Vol. US 7033969*, 2006.

[5]   R. B. Scholl, A.; Stephani, G.*, Vol. DE 10160640 C2*, 2003.

[6]   C. Kostmann, in *Strategien zur aktiven Geräuschminderung von Bauteilen und Komponenten im Maschinen- und Anlagenbau*, Fraunhofer-Institut für Fertigungstechnik und Angewandte Materialforschung, Dresden, 2004.

[7]   J. M. Cowley, *Diffraction Physics*, third ed., Elsevier, 1995.

[8]   F. Bretschneider, e. al*, Vol. DE 19929760 C2*, 2003.

[9]   F. Bretschneider, e. al.*, Vol. DE 10003175 C2*, 2002.

[10]   *Stahl und Eisen. Gütenormen 5*, 2002.

[11]   M. Valentini, G. Groppi, C. Cristiani, M. Levi, E. Tronconi, P. Forzatti, *Catalysis Today* 2001, *69*, 307.

[12]   S. Zhao, J. Zhang, D. Weng, X. Wu, *Surface and Coatings Technology* 2003, *167*, 97.

[13]   http://www.physik.tu-muenchen.de/antares/, 2007.

[14]   http://www.iupac.org/goldbook/E02170.pdf, 1994.

[15]   K. Lorenz, E. Lehmann, E. Steichele, P. Vontobel, *Nuclear Instruments and Methods in Physics Research Section A: Accelerators, Spectrometers, Detectors and Associated Equipment* 2005, *542*, 95.

[16]   J. C. Domanus, G. Bayon, *Practical Neutron Tomographie*, Kluwer Academic, Dordrecht, 1992.

[17]   M. Mühlbauer, E. Calzada, B. Schillinger, *Nuclear Instruments and Methods in Physics Research Section A: Accelerators, Spectrometers, Detectors and Associated Equipment* 2005, *542*, 324.

[18]   J. Wiehl, C. D. Vogt, *MTZ* 2003, *2*, 112.

[19]   S. Ebener, U. Zink, in *FAD Conference*, Dresden, 2004.

[20]   M. Wadsworth, in *Arvin Meritor*, Arvin Meritor, 2001.

Chapter 5

5   Tomography: Comparison of neutron and x-ray technology for the visualization of features in emission catalysts

5.1 ABSTRACT

Tomography experiments (X-ray tomography and neutron tomography) are a non destructive technique to image and investigate microscopic and macroscopic features of hollow sphere structures used as car exhaust catalysts. The wall and coating thickness of single spheres were determined with X-rays whereas the distribution of coke inside a real catalyst was studied with neutron tomography. These results can be used to improve the properties of the structure, washcoat thickness or favor flow characteristics.

5.2 INTRODUCTION

After decades of using the well established x-ray computed tomography for mainly medical reasons, another technique, neutron tomography, evolved in the last years [1,2]. Various applications in fields outside medicine are studied with x-ray technology, ranging from examinations of mummies to explosives detection systems [3]. Neutron tomography which requires a much higher energy from thermal or cold neutrons is mainly based in research nuclear reactors or at synchrotrons. Its main task is the identification of different materials useful in material science. Besides the differences in resolution and experimental setup, the theory of both techniques differs significantly. Neutrons interact by scattering or absorption with atomic nuclei while X-rays interact with the electrons surrounding a nucleus. Improving the resolution of both techniques makes this experiments interesting for industrial applications as well. Non-destructive testing can be a fast and cheap way to proof and improve the quality of standard parts or modern comforts [4].

This work focus on two different non-destructive technologies for the investigation of car catalyst structures and single coated hollow spheres used in these application. Different

tomography techniques, cold neutron absorption imaging and x-ray imaging are compared. After explanation of the theory of both technologies, these results were used to get insights in the macroscopic and microscopic structure of the investigated samples.

Theory x-ray tomography (µ-CT)

The interaction of phonons with matter in the X-ray regime is dominated by the photoelectric effect, Compton scattering and pair production. These different mechanisms have implications for CT image contrast and artifacts owing to beam hardening and scatter contamination. X-ray photons with less than 25 keV interact mainly via the photoelectric effect, and their attenuation varies approximately with E^{-3}. At higher photon energies Compton scattering is the main mechanism of X-ray interaction and the attenuation varies with $E^{-0.5}$. This explains why a greater tissue contrast can be achieved at low photon energies. For tomographic measurements with an X-ray beam with a certain photon energy (E), the thickness of the investigated object should be in the order of $D = 2/ \mu(E)$ to get an optimal signal-to-noise ratio [5].

Theory neutron tomography

In neutron radiography, the different attenuation of the neutron beam on different paths through the object causes the so called absorption contrast. The attenuation of the neutron beam by a certain material with the thickness d and the density ρ is described by the exponential attenuation law. Generalized, for samples consisting of different materials with variable densities, the intensity I(d) behind the object is given by

$$I(d) = I_0 \exp\left(-\int_0^d \mu(x)\rho(x)dx \right),$$

where I_0 is the intensity of the incident beam and μ the mass attenuation coefficient of the material. Variations in the density of a material or interfaces between different materials cause variations in the intensity at the detector, which is the absorption contrast [6].

5.3 EXPERIMENTAL

5.3.1 X-ray Tomography setup

An X-ray tomographic microscope (Scanco μ-CT 20) with a spatial resolution of 8 μm was used to study the samples. The system is fully automated and working with a fan-beam of X-rays. Projections (600) are taken over 216 ° (180 ° plus 1/2 the fan angle on either side). A standard convolution-backprojection procedure with a Shepp and Logan filter is used to reconstruct the CT images. Samples with diameters below 7 mm can be measured. The measuring system is schematically represented in Figure 1. The object is mounted on a turntable that can be shifted automatically in the axial direction. The radiation from an X-ray tube is focused through slits at the tube aperture. A small X-ray tube (KEVEX PXS5) is used as a source. Its focal spot has a nominal diameter of 10 μm. The filtered (0.3 mm Al) 40 kV X-ray spectrum is peaked at 25 keV, allowing excellent metal versus air contrast due to the pronounced photoelectric effect. This energy setting is sufficient to penetrate objects up to 10 mm in diameter. After reconstruction, the 3D object is created and analyzed to receive the aimed values. [7]

The used fan beam geometry brings simplicity of operation and reconstruction in comparison to the direct 3D cone beam reconstruction, by measuring a stack of 2D CT slices in order to get a 3D representation of the object.
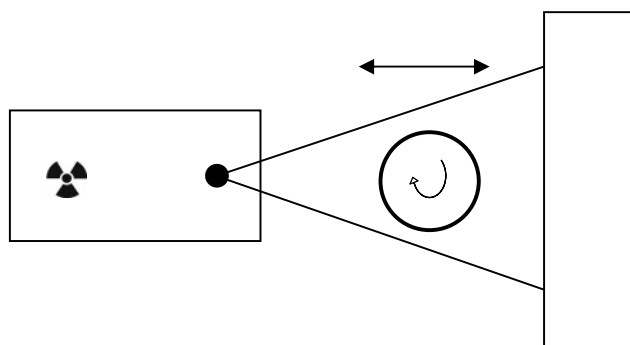
Figure 1: Schematic layout of the setup for X-ray imaging.

5.3.2 Neutron Tomography measurement setup

The experiments were performed at the cold neutron radiography facility ANTARES at FRM-II, Munich. A schematic layout of the experimental layout is shown in fig. 2. An aperture wheel allows introducing pinhole apertures in 14m distance from the sample position in the beam. With these apertures, the L/D ratio can be changed from 400 to 14000. Next to the aperture wheel a multifilter was installed, which allows the utilization of different crystal filters to reduce gammas, epithermal neutrons or to modify the neutron spectrum. At the sample position, the sample is placed on a rotary table that is mounted on a manipulator to position the sample in the beam. A LiF-scintillator converts neutrons into visible light, which is detected by a CCD camera with 2048 x 2048 pixels. The maximum usable beam diameter is limited by the size of the scintillator which has a width and length of 26 cm. During a routine tomography, the sample is rotated in 200 to 800 angular steps from 0° to 180°. The main properties of the beam line are a neutron-flux intensity of 10^8 cm^{-2} s^{-1} for L/D=400. For the tomographic measurement an L/D ratio of 800 and a sample-detector distance of 8 cm was used, leading to an exposure time of 7 s per radiography.
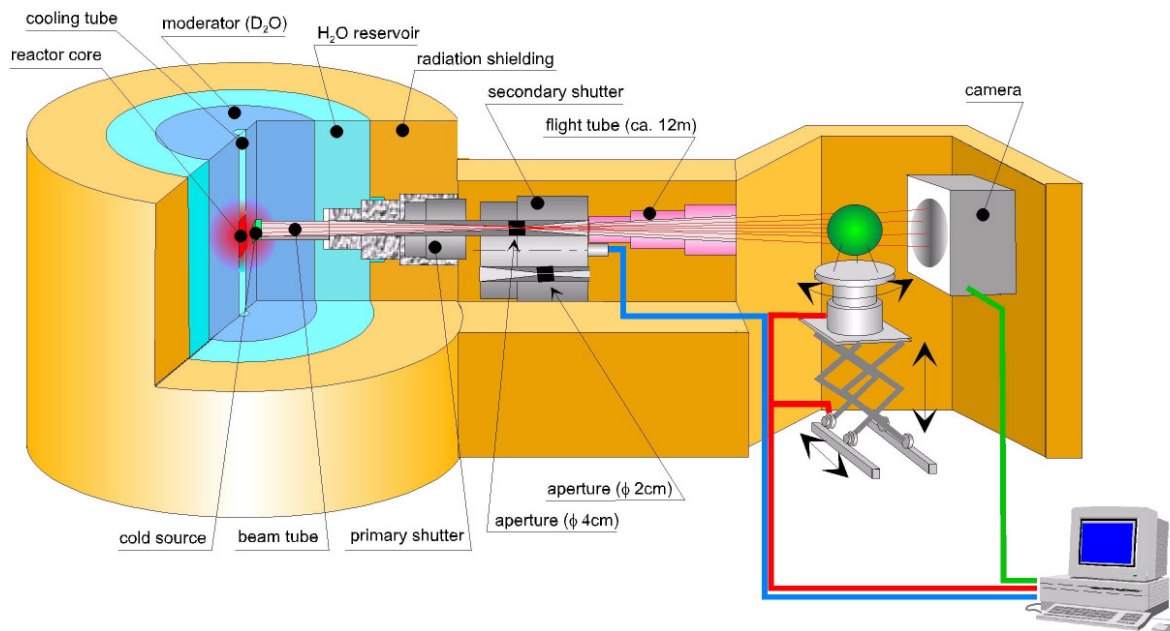
Figure 2: Schematic layout of the setup for neutron tomography.

In neutron tomography, several radiographies of an object are made under different angles. This set of projections can be used to reconstruct a 3D model of the object in a computer. The grey value of a pixel corresponds to the attenuation of the neutron beam at this position in the object. Like this the inner structure of an object can be visualized and analyzed. The attenuation coefficient is material specific. The assignment of colors to different materials permits the clarification of different materials inside one structure.

5.4 RESULTS

Both techniques, neutron and x-ray tomography are rather new techniques. They are applied for non-destructive testing in various fields. The potential of scanning tomographies is demonstrated in the following application. The investigation of hollow sphere diesel oxidation catalysts will provide insights in coke deposition, washcoat thickness, as well as microscopic and macroscopic detailed views measured by neutron and x-ray tomography. The application

involves the evaluation of stainless steel hollow spheres used in support structures for new car catalysts.

5.4.1 X-ray tomography

Determination of washcoat thickness

Hollow spheres with an average of 3 mm diameter were investigated.
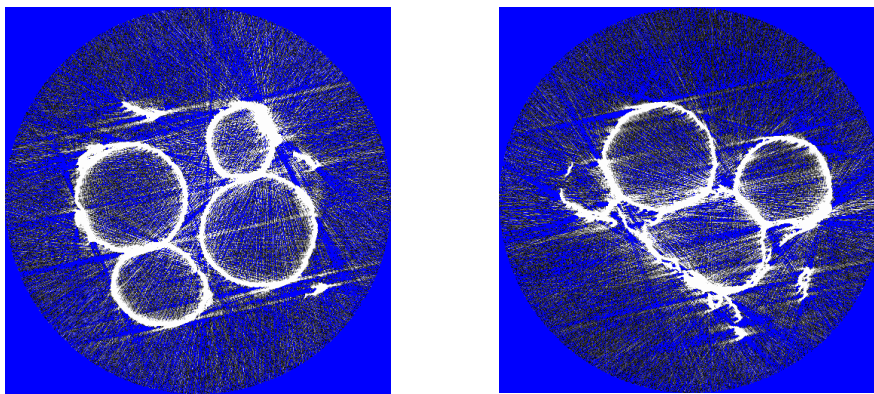
Figure 3: fan beam recordings of coated (left) and uncoated (right) hollow spheres

The figure above shows radiographies of hollow spheres with an average diameter of 3 mm. Both recordings show cuts through spheres with coating on the left side and the right side displays the image of spheres without coating. The thickness of the metal sphere wall was calculated to 0.137 mm with coating and 0.126 mm without coating. This leads to a washcoat thickness of 11 μm.

Topology of the surface of hollow spheres

In order to compare the morphology of coated and uncoated hollow spheres, the 3D reconstruction was done.
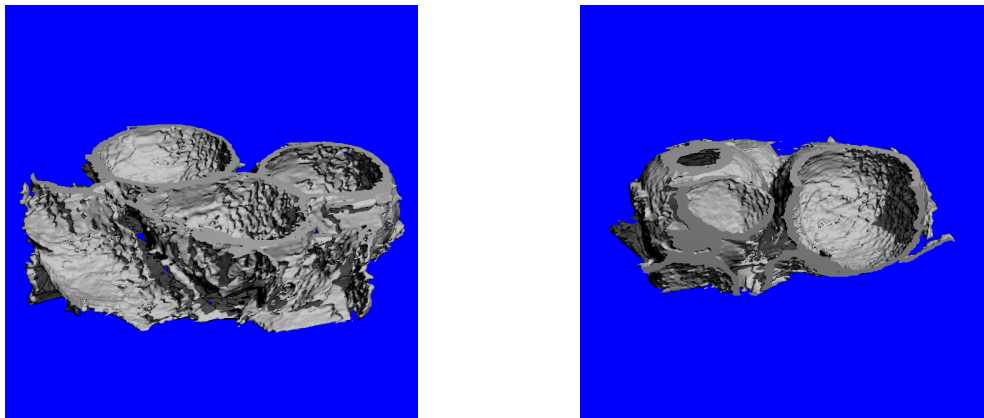
Figure 4: Reconstructed hollow spheres recorded with x-ray tomography

A closer look at the outer surface reveals details of the surface. Figure 4 on the left side with rough surfaces stands for a hollow sphere without coating, whereas the hollow sphere with coating seems to have a much smoother surface.

Visualization of 6 mm hollow spheres

A hollow sphere with a diameter of 6 mm was investigated.
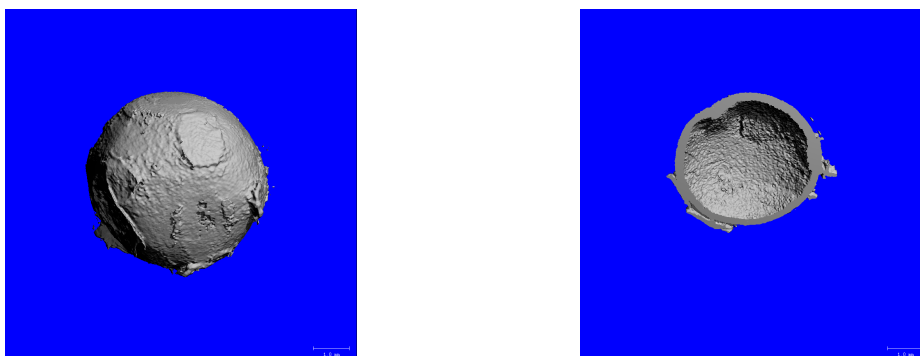
Figure 5: Reconstructed 6 mm hollow sphere recorded with x-ray tomography

A hollow sphere of 6 mm diameter was investigated with µ-tomography with and without coating. Above, the hollow sphere is displayed with coating. A cut through the reconstructed image proofs the inner empty space of the sphere. The volume of the metal hollow sphere was

23.7974 mm³ without coating and 23.9966 mm³ with alumina coating. The thickness of the metal wall was determined to 0.249 mm without and 0.2581 mm with coating, resulting in a washcoat thickness of 9.1 µm. Both measurements were carried out under the same conditions. Small errors are due to artifacts and Gaussian filtering.

5.4.2 Neutron tomography

A used car catalyst with a support structure consisting of 6 mm hollow spheres was investigated with neutron tomography. The neutron tomography was recorded of the macroscopic catalyst structure in order to get information on defects caused by the manufacturing process and to display the distribution of coke.
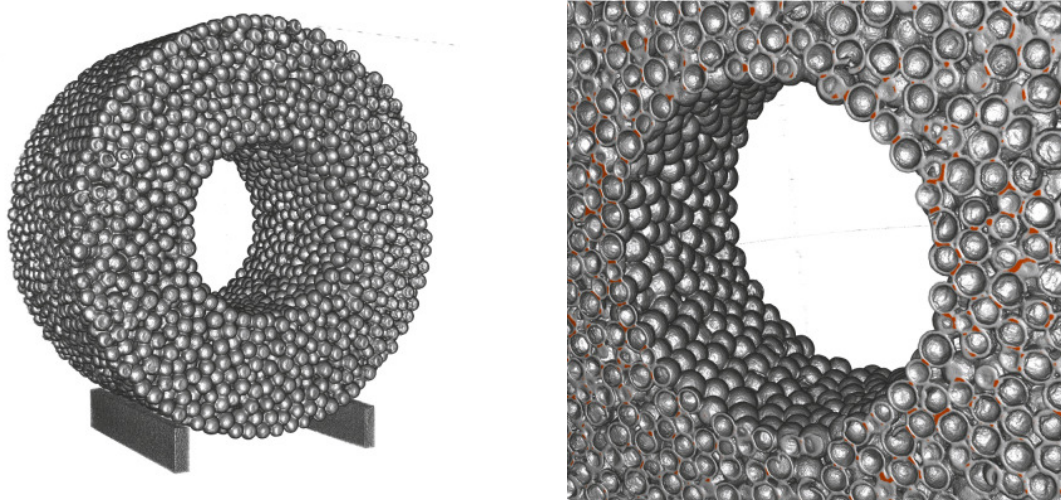
Figure 6: Reconstructed hollow sphere structure recorded with neutron tomography: total view of car catalyst (left), axial cut with visualization of deposits (right)

The investigated catalyst was used in an engine test bench to test the activity under real conditions. Figure 6 (left) above shows the calculated 3D structure. Both materials, steel hollow spheres and coke deposits are shown in an axial cut (fig 6 right) through the structure. The deposits are visible in channels and spaces between packed hollow spheres. After removing

the material of the hollow spheres in the calculation, only deposits inside the macroscopic structure are left (fig 7). The coke deposit can be seen throughout the catalyst. However the distribution is not uniform.
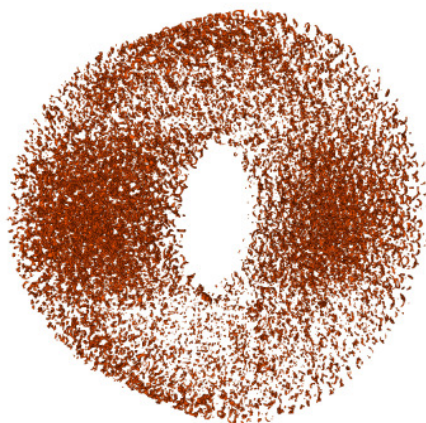
Figure 7: Visualization of deposits inside the hollow sphere structure

5.5 DISCUSSION

Macroscopic and microscopic visualization are valuable tools for non-destructive testing. X-ray and neutron tomography were used to display interesting features of a new car catalyst. Hollow spheres act as oxidation catalyst and particle trap. Both techniques complete each other in different applications. X-ray tomography is the tool to visualize single hollow spheres and due to its high resolution detailed information can be obtained about the washcoat. Single hollow spheres can be scanned to visualize the interior of hollow spheres and to show results about material deposits or deformation. Hollow spheres with a diameter of 3 mm were investigated and an average wall thickness of 137 µm for coated hollow spheres and 126 µm for uncoated hollow spheres was found. The washcoat was calculated to 11 µm. Further investigations with 6 mm hollow spheres lead to a washcoat thickness of 9 µm. The morphology of coated and uncoated spheres can be compared too. X-ray imaging proofs a rough surface of uncoated spheres (µm range) whereas coated spheres exhibit a smooth surface.

Neutron tomography with lower resolution is useful for the visualization of the macroscopic structures. The 3D reconstruction of a hollow sphere structure, used as oxidation catalyst in an engine test bench, was cut in certain levels to check for deformations and the fade-out of hollow spheres to display deposits between them. These deposits are coke from testing the catalyst in an engine test bench.

5.6 CONCLUSIONS

Non destructive investigations with X-ray tomography and neutron tomography are valuable tools for microscopic and macroscopic hollow sphere structures used as car exhaust catalysts. Determination of the wall and coating thickness of single spheres allow the improvement of the production procedure as well as the evaluation for quality control. Further, the distribution of coke inside a real catalyst can be studied with neutron tomography. The resulting distribution can lead to adjustments of gas flows to achieve homogeneous conditions.

5.7 ACKNOLEDGEMENTS

5.8 REFERENCES

[1] A.A. Pitsillides, Bone 37 (2005) 810

[2] F. Fiori, Meas.Sci.Technol. 17 (2006) 2479

[3] Neutron Imaging & Activation Group (NIAG), Paul Scherrer Institut, 2006, Villingen

[4] G.A. Appleby, Nuclear Instruments and Methods in Physics Research A 564 (2006) 424

[5] E.L. Ritman, Annu. Rev. Biomed. Eng. 6 (2004) 185

[6] K. Lorenz, Nuclear Instruments and Methods in Physics Research A 543 (2005) 95

[7] P. Rüegsegger, Calcif Tissue Int 58 (1996) 24

Chapter 6

6 Effect of chromium migration from metallic supports on the activity of (diesel) exhaust catalysts

6.1 ABSTRACT

The influence of chromium migration from the metal support into the washcoat of diesel exhaust catalysts on the catalytic activity for the oxidation of NO and CO was investigated. Two different stainless steel supports (Fe-Cr-Ni and Fe-Cr-Al) were compared with a standard catalyst using a monolithic structure of cordierite in a flow reactor. The initial rates were determined before and after a thermal aging process. The extensive loss of activity for the NO oxidation after aging of the Fe-Cr-Ni support was assigned to the migration of chromium from the metal bulk phase into washcoat, which could be verified by XPS and SEM measurements. In the contrary, for the presence of aluminium in the Fe-Cr-Al steel alloy formed a protective alumina barrier, which inhibited the degradation of the catalyst after aging by blocking the migration of chromium to the surface

6.2 INTRODUCTION

In diesel cars catalytic converters for the oxidation of CO and residual hydrocarbon emissions are necessary to comply with current emission legislations. Typical diesel oxidation catalysts are based on platinum as active component for the oxidation of CO, NO and hydrocarbons and supported ceramic or metallic monoliths [1]. Recently, support structures based on stainless steel hollow spheres were proposed for future applications, which allow the combination of different functionalities such as catalysis with noise reduction. Most studies of diesel oxidation catalysts have investigated reaction mechanisms and tried to improve the catalytic properties, whereas the diffusion of elements such as Cr from the metallic support into the active noble metal and the resulting deactivation of the catalysts have not been studied in detail [2]. In general the following processes for deactivation of the exhaust catalyst have been reported: (i)

loss of metal surface due to sintering of Pt after long-term operation at high temperature (thermal deactivation) [3], (ii) accumulation of poisons such as Ca and P arising from the lubricant oil on the surface of the active sites [4], (iii) formation of sulfates from sulphur species in the fuel [5] [6], (iv) coking [7] and (v) the migration of poisons from the support into the active phase [8]. Several studies have shown that deactivation depends strongly on the combination of parameters such as time, temperature, atmosphere, support, and catalyst composition [9]. The support material used in these studies consisted of ceramic and stainless steel structures (Fe-Cr-Ni and Fe-Cr-Al). It is known that Fe-Cr-Ni steels contain elements, such as e.g. chromium [10], which can migrate from the bulk phase of the metal support onto the surface in high temperature environments. Therefore, special alloys such as Fe-Cr-Al were developed, which prevent this effect by forming a protective alumina layer on the surface in a pre-oxidation step [11].

In the study presented Pt-based oxidation catalysts (DOC) on metallic hollow sphere structures and a ceramic monolith were subjected to thermal aging under laboratory conditions. The activity was determined from the rate of NO oxidation and the light-off temperature for the CO oxidation. SEM was used to analyze the washcoat thickness and to detect the concentration of chromium on the surface, which was further confirmed by XPS measurements.

6.3 EXPERIMENTAL

6.3.1 Catalysts

For catalyst A (21 mm x 25 mm) and catalyst B (21 mm x 28 mm) sintered hollow sphere supports (sphere diameter of 3 mm) made of Fe-Cr-Ni and of Fe-Cr-Al stainless steel, respectively, were used (see table 1). For catalyst C (21 mm x 25 mm) a ceramic monolith (cordierite 400 cpsi) was used as support. The structures were coated with a standard washcoat based on Al_2O_3 and impregnated with Pt (loading 100 g/ft³), a formulation typically used for diesel oxidation catalysts [12] [13].

Table 1: Composition of the metallic support structures [14]

	Cr	Ni	Mn	Si	C	S	P	Al	O	Fe
catalyst A	24-26	19-22	<2	1,5-2,5	<0,2	0,03	0,045		<0,1	balance
catalyst B	19-22		<1	<1	<0,1	0,03	0,045	5		balance

6.3.2 Catalytic test reactions

The oxidation of NO and CO with O_2 was studied in a flow reactor and the concentration of products was continuously analyzed by IR spectroscopy (FTIR Thermo Electron Corporation NEXUS, OMNIC QuantPad software) using a heated, low volume multiple-path gas cell [15]. The reactions were carried out using a gas stream consisting of 4000 ml/min N_2 (carrier gas), 50 ml/min O_2 and 4 ml/min NO or CO, which corresponds to a NO/CO concentration of 1000 ppm and an oxygen concentration of 2.5 %. The space velocity over the catalyst was 70000 h^{-1}. During the experiments the temperature was increased from room temperature to 550 °C using an increment of 1 °C/min while continuously monitoring the concentration of products and reactants. Aging of the catalysts was carried out in the reactor at 800 °C for 48 h under synthetic air flow.

6.3.3 X-ray photoelectron spectroscopy (XPS)

Photoelectron spectra were recorded on a Leybold LH10 system using the X-ray radiation of Al (Kα 1486.6 eV) to eject the inner electrons from the core orbitals of the atoms in the sample [16]. The analysis chamber was operated under ultrahigh vacuum with a base pressure close to 4 x 10^{-9} mbar. The binding energies were referenced to the C1s peak at 284.9 eV due to adventitious carbon. The intensities of the following peaks were used for quantitative analysis:

Al 2s, O 1s, C 1s, Fe 2p³, Cr 2p³, Pt 4f, and Pt 4d. Peak areas were determined using Shirley background subtraction. Sensitivity factors S from Briggs and Sheah [17] were used.

6.3.4 Scanning electron microscopy (SEM)

Investigations were carried out on a JEOL 500 instrument with an accelerating voltage of 25 kV. Energy dispersive X-ray spectroscopy was used for the chemical characterization of Cr. The sample investigation is based on interactions between electromagnetic radiation and matter, analyzing X-rays emitted by the matter in this particular case. Each element has a unique atomic structure allowing x-rays that are characteristic of an element's atomic structure to be uniquely distinguished from each other.

6.4 RESULTS

6.4.1 Effect of the aging process on NO and CO activity

The activity of the three catalysts for the oxidation of CO and NO was studied. A typical conversion profile over catalyst B is shown in Figure 1 for the oxidation of CO (dots) and NO (triangles), the latter is limited by the thermodynamic equilibrium between NO and NO_2 (values calculated indicated by diamonds). Therefore, the NO conversion increases with temperature and after the NO_2 concentration reaches the thermodynamic equilibrium the conversion follows the decrease in the NO_2 equilibrium concentration with increasing temperature [18-24]. In contrast the CO conversion is not limited by equilibrium therefore the conversion reaches 100% [25].
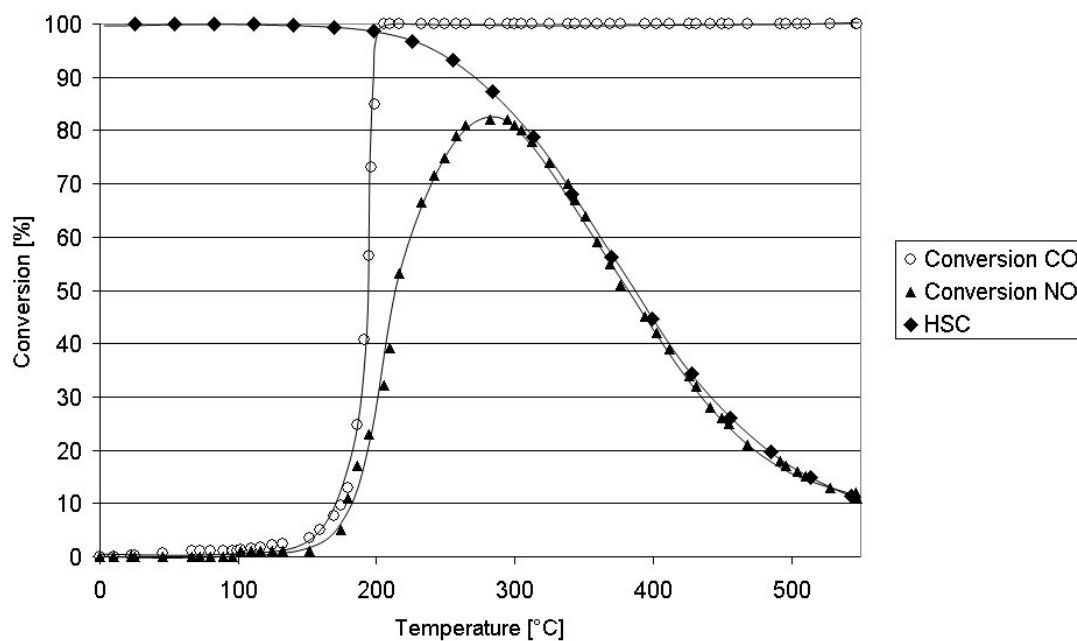
Figure 1: Typical conversion profile for the oxidation of NO and CO

The (differential) rate for the oxidation of NO at 200 °C and the light-off temperature for the CO oxidation (temperature for 50 % CO conversion) were used to compare the activity of the catalysts. The rates for the oxidation of NO of monolith and hollow sphere catalysts before and after aging the catalyst structures are compared in Figure 2.
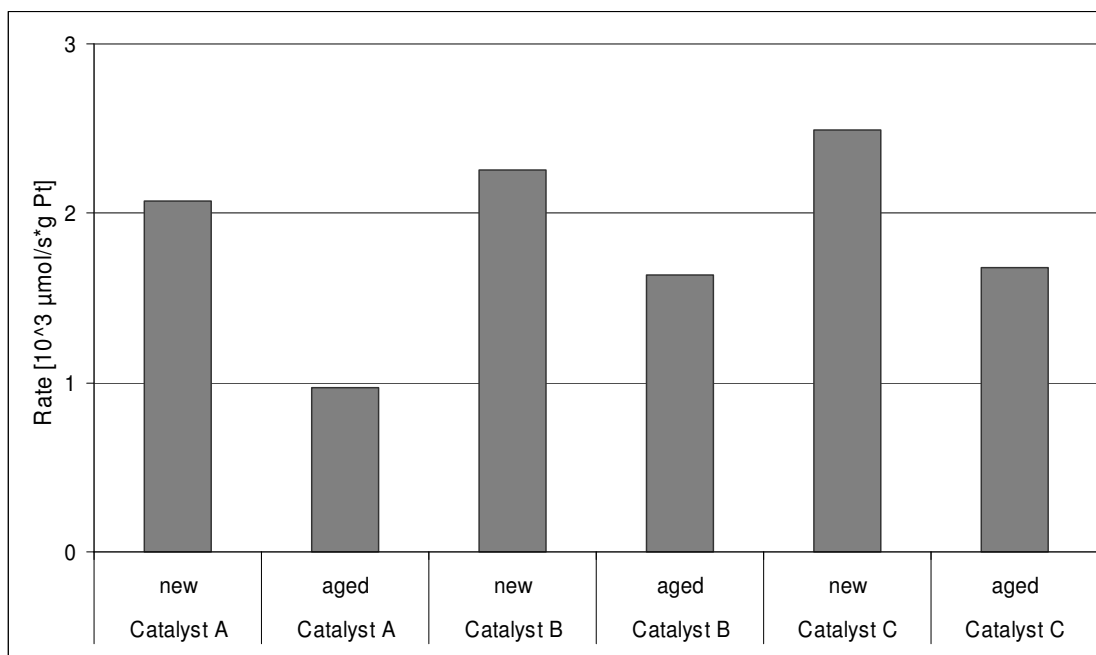
Figure 2: Rate of NO oxidation at 200 °C

Catalyst A showed the lowest activity for NO oxidation (rate 2.07×10^{-3} µmol/(s*g Pt)) followed by Catalyst B (2.26×10^{-3} µmol/(s*g Pt)) and Catalyst C (2.50×10^{-3} µmol/(s*g Pt)). After thermal aging at high temperature the activity for the NO oxidation generally decreases due to sintering of Pt particles on the surface. Catalyst C and B showed almost the same activity after aging (decrease 27 % and 32 %, respectively), whereas the activity of catalyst A significantly decreased (53 % loss of activity).

The light-off temperatures for the catalysts before and after thermal aging are compared in figure 3 [26-28].
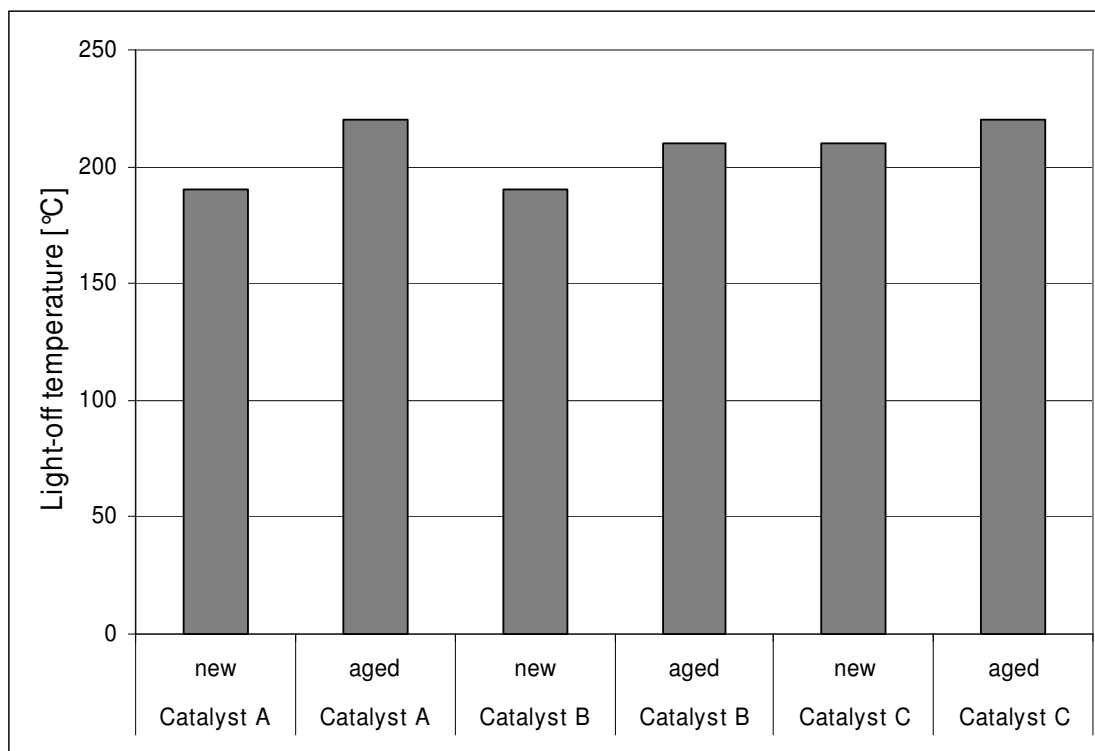
Figure 3: CO light-off temperature

Catalysts on the hollow sphere structures (catalysts A and B) showed a lower light-off temperature (190 °C) compared with the cordierite monolith support (210 °C). After the aging the light-off temperature increased for catalyst A to 220 °C, for catalyst B to 210 °C and for catalyst C to 220 °C.

6.4.2 Testing for mass transport limitations

The influence of mass transfer through the laminar film on the catalyst surface (film diffusion) was confirmed by measuring the conversion of NO as function of the flow, while maintaining constant residence time by increasing the catalyst length (shown in figure 4).
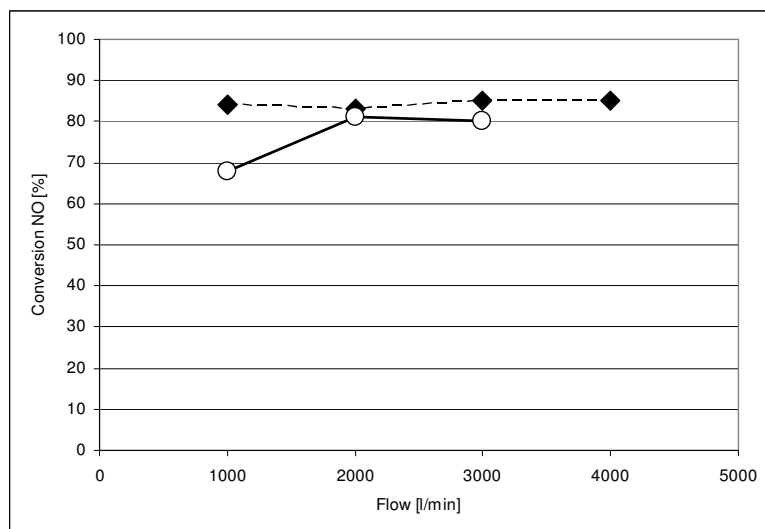
Figure 4: Determination of film diffusion: hollow sphere structure and monolith

In the flow range studied (1000 – 4000 l/min) a constant NO conversion was observed, indicating that the mass transport in the film did not influence the rate of the reaction over the hollow sphere structures (indicated by diamonds). However, film diffusion limitation occurred for monolithic structures (indicated by dots).

6.4.3 Washcoat thickness for hollow sphere supports

Sintered metal foils consisting of the same alloys as the hollow sphere supports (Fe-Cr-Ni and Fe-Cr-Al) were coated with an alumina based washcoat and the thickness of the oxide layer was measured by scanning electron microscopy. The results are compared in Figure 5.
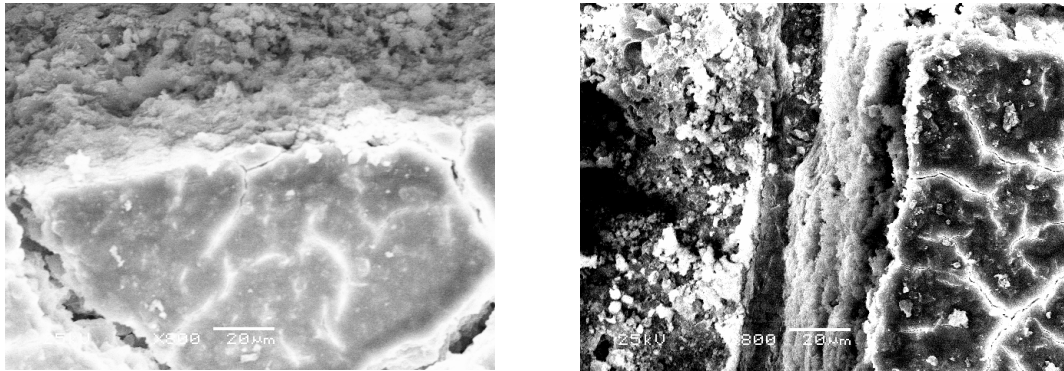
Figure 5: SEM of washcoat surface on Fe-Cr-Ni foil and on Fe-Cr-Al foil

For both supports a washcoat thickness of 20 µm was determined by SEM. Moreover, both surfaces revealed distinct cracks [29], which result from the thermal treatment during calcination.

6.4.4 Influence of chromium on the surface of Fe-Cr-Ni stainless steel

The concentration of the element Cr on the foils coated with the alumina based washcoat was determined by energy dispersive X-ray spectroscopy scanning electron microscopy [30-33].
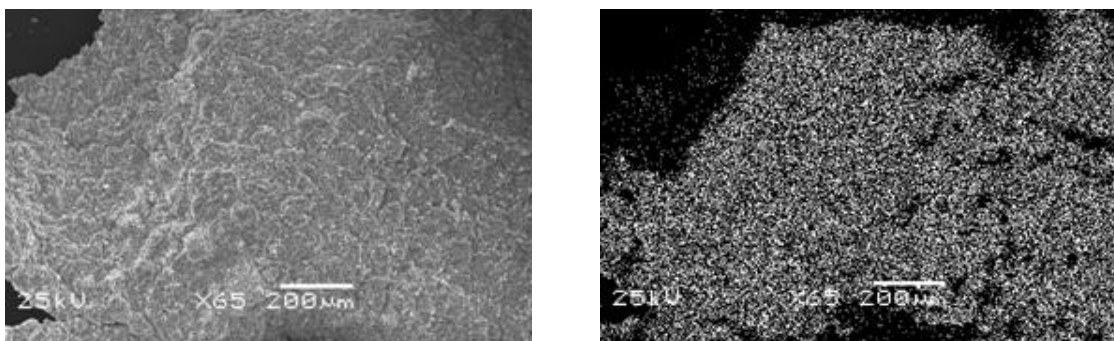
Figure 6: SEM and EDX mapping of Cr after aging

The SEM of the hollow sphere structure of catalyst A after aging and EDX for the homogeneous distribution of Cr, visualized by the Cr mapping, is compared in Fig. 6, which indicates that Cr is distributed over the whole surface of catalyst A. Catalyst B did not reveal Cr on the surface.

The verification of the migration of Cr onto the surface during the thermal aging process XPS was recorded for the sintered foils of catalyst A and B, after coating with the washcoat and after the aging process to gain information on structural changes, with a special emphasis on the Cr concentration.

For both model catalysts a similar composition of the washcoat was observed before aging. The XPS of the pre-oxidized foil of catalyst B and the foil of catalyst A are shown in Fig 7.
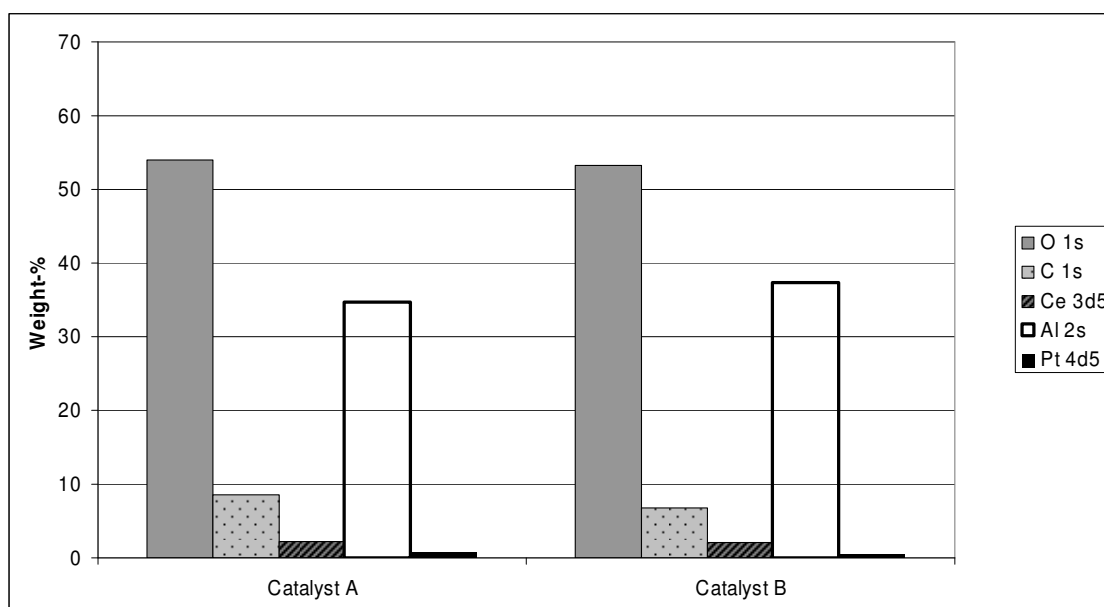
Figure 7: Weight-% of the washcoat compositions of catalyst A and catalyst B

The formation of a thin alumina film (whisker forming) on the surface of the Fe-Cr-Al alloy during the pre-treatment was proven by color change of the surface from grey to light-blue. The

preferred phase on the surface of Fe-Cr-Al at high temperature is alumina, in contrast to chromia for Fe-Cr-Ni alloys [34-35].
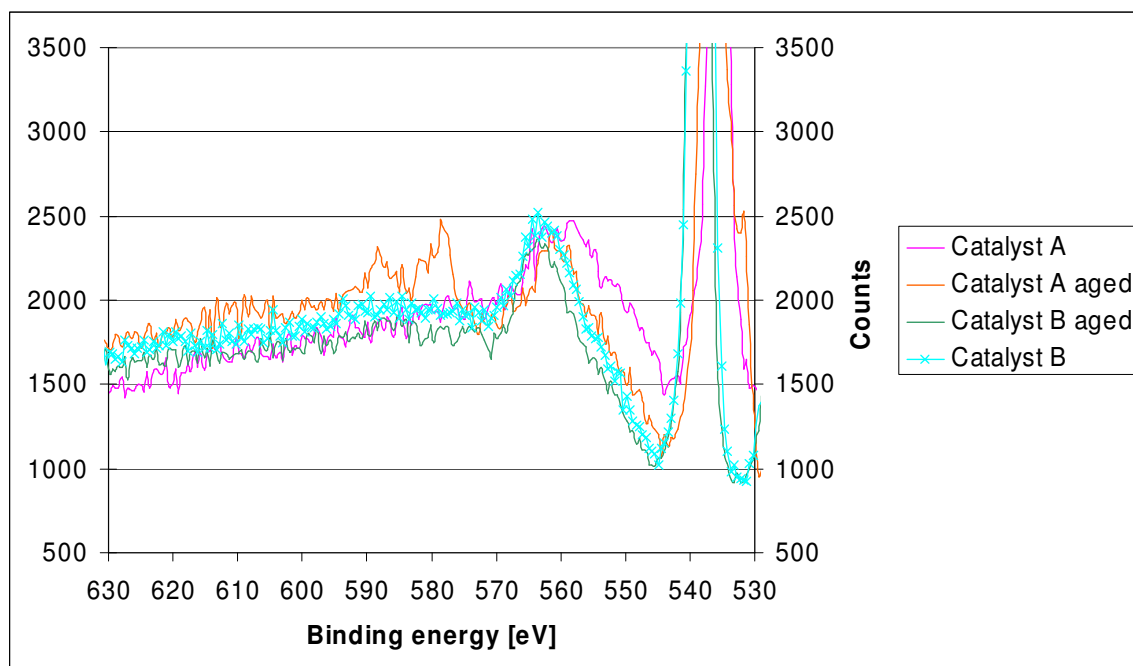
Figure 8: XPS for catalyst A and B before and after aging

The XPS for catalyst A and B before and after thermal aging are compared in Fig. 8. The XPS peak at 580 eV confirms the presence of Cr on the surface of the aged Fe-Cr-Ni catalyst, whereas on the fresh catalyst A, as well as on the fresh and aged catalyst B Cr could not be detected on the surface.

6.5 DISCUSSION

The activity of both oxidation catalysts based on Pt supported on the hollow sphere structures for the oxidation of NO and CO was comparable to the reference material (Pt on a traditional monolith based on cordierite) and to the data reported in the literature [36]. No film diffusion influence was found for hollow sphere supports, which is a big advantage compared to the film diffusion limitation that was found for monolithic structures. Tronconi [37-39] has stated that monolithic catalysts in industrial applications typically run under external mass transport limitation.

Thermal aging at 800 C was carried out to simulate the deactivation of the catalysts during the long-term vehicle operation. For the catalysts based on the hollow sphere structures as well as for the catalyst on the ceramic monolith a decrease in the activity for the oxidation of CO and NO was observed. For CO oxidation the light-off temperature increased from 190-200 °C before aging [40] to 210-220 °C, which is in accordance with literature [41].

For the Pt catalysts supported on the metal spheres as well as for Pt supported on the cordierite monolith the activity for the NO oxidation decreased significantly after the thermal aging. For the Fe-Cr-Al support (catalyst B) and for the cordierite monolith (catalyst C) the activity decreased about 30% after the thermal aging, while for the catalysts on the Fe-Cr-Ni support (catalyst A) a decrease of the rate in the NO oxidation of more than 50% was observed. Among the reasons for deactivation already mentioned in the introduction only the migration of elements from the bulk phase of the support onto the catalysts surface can account for this behavior.

The diffusion/migration of elements form the steel alloy such as Cr into the washcoat or even into active noble metal, which results in a deactivation of the catalyst appears to be feasible under high temperature conditions. Therefore, special alloys such as Fe-Cr-Al were developed, which prevent this effect by forming a protective alumina layer on the surface in a pre-oxidation step [11]. The presence of Cr after aging of the Fe-Cr-Ni support (catalyst A) was verified by

XPS, while on this catalyst before aging and on the Fe-Cr-Al supported catalyst (catalyst B) Cr could not be detected before and after thermal aging. A further proof for the presence of Cr was the homogeneous distribution of Cr on the surface of catalysts A after aging indicated by EDX mapping. Both experiments indicated that Cr was diffusing from the stainless steel support (Fe-Cr-Ni) through the washcoat to the surface for catalyst A [42-45]. The interaction between the chromium and the oxygen terminated alumina film results in the formation of chromium oxide on the surface.

In principle Cr diffusion should be also possible from the Fe-Cr-Al alloy used in catalyst B. The difference between the Fe-Ni-Cr and the Fe-Cr-Al alloy is that at high temperatures (~1000 °C) the Fe-Cr-Ni alloy forms a Cr_2O_3 phase on the surface, whereas the Fe-Cr-Al alloy forms a dense Al_2O_3 phase which prevents further migration of Cr [46, 11] [47]. After the thermal pretreatment of catalyst B, the color of the alloy changed from grey to light-blue, which indicates the formation of the protective alumina layer on the surface [46, 11]. The rate for the oxidation of NO was determined for an aged monolithic structure, which was poisoned before by dipping in a Cr-solution. This experiment did not show any activity for the oxidation of NO. Therefore, Cr is not an active component for the oxidation of NO.

An explanation for the influence of Cr on the surface of the Fe-Cr-Ni support might be given in analogy to metalcarbonyle reactions. NO is a stronger acceptor of backbonding electrons of the metal than CO. If NO bonds to the metal, the additional electron of the NO radical is transferred completely to the metal atom, therefore, a nitrosyl ion is formed which is isoelectronic to the CO molecule. The extra electron provided by the 3-electron donor NO to the metal results in a stronger backbonding into molecular NO orbitals. In contrast, the 2-electron-donor, CO results in a smaller ability of backbonding which leads to a weaker metal ligand interaction. In mixed carbonyl nitrosyl metal complexes only the carbonyl complex is exchanged by the addition of stronger ligands, like PR_3 or NR_3 [48].

If Cr is present on the surface, only CO can be oxidized to CO_2, whereas NO can only bond to the surface without further reaction. Therefore the oxidation of CO is not influenced by Cr on the surface, but the NO oxidation rate is reduced because less active sites are available.

6.6 CONCLUSION

This paper has demonstrated that stainless steel hollow sphere structures are a promising alternative to monolithic catalysts as diesel emission catalysts for NO and CO oxidation. Similar catalytic activity was reached in the oxidation of NO to NO_2 and CO to CO_2 with hollow sphere supports compared to the traditional corderite monolith supports. However caution is necessary in case of constant high temperature applications, which can lead to the migration of chromium from the support through the washcoat to the surface which causes a loss of activity for Fe-Cr-Ni alloys. Improvement of the stainless steel, changing the support structure to Fe-Cr-Al with low aluminum content, resulted in the growth of a protective alumina barrier layer during the pre-oxidation process. The metal hollow sphere structure made of Fe-Cr-Al can compete with the monolithic catalyst as support for NO and CO oxidation as Pt/Al_2O_3 diesel oxidation catalysts.

6.7 ACKNOWLEDGEMENT

6.8 REFERENCES

[1] H.J. Stein, Appl.Catal.B: Environ. 10 (1996) 69

[2] J.E. Johnson, Appl. Catal. B: Environ. 10 (1996) 117

[3] G. Mabilon, Stud.Surf.Sci.Catal. 71 (1991) 569

[4] J. Andersson, Applied Catalysis B: Environmental 72 (2007) 71-81

[5] A.F. Lee, J.Catal. 184 (1999) 491] [D.Y. Murzin, Fuel 83 (2004) 395-408

[6] D.Y. Murzin, Fuel 83 (2004) 395-408

[7] S. Albertazzi, Appl. Catal. A: Gen 247 (2003) 1-7

[8] A.M. Efstathiou, Applied Catalysis B: Envrionmental 54 (2004) 237-250

[9] D. Lieftink, Applied Catalysis B: Environmental 74 (2007) 251-260]

[10] H. Kurokawa, Solid States Ionics 168 (2004) 13-21

[11] M. Montes, Applied Catalysis B: Environmental 78 (2008) 166-175

[12] M. Valentini, *Ca*talysis Today 69 2001 307

[13] S. Zhao, Surface and Coatings Technology 167 2003 97

[14] Stahl und Eisen. Gütenormen 5, **2002**.

[15] P. Hauck, Dissertation 2007, chapter 4

[16] G. Moretti, in: Handbook of Heterogeneous Catalysis Vol.2, editors G. Ertl, H. Knözinger and J. Weitkamp VCH-Wiley 1997 632-641

[17] C.Wagner, in: Practical surface analysis Vol 1,2[nd], editors D. Briggs and M.P. Sheah Wiley 1990

[18] L. Ilieva, Applied Catalysis B: Environmental 65 (2006) 101-109

[19] R. Burch, Applied Catalysis B: Environmental 15 (1998) 63-73

[20] R. Burch, Journal of Catalysis 176 (1998) 204-214

[21] P.J.Schmitz, Applied Catalysis B: Environmental 67 (2006) 246-256

[22] L. Olsson, J.Phys.Chem.B 103 (1999) 10433-10439

[23] K. Eguchi, Applied Catalysis A: General 226 (2002) 23-30

[24] S. Kureti, Journal of Catalysis 229 (2005) 480-489

[25] R. Burch, Applied Catalysis B: Environmental 15 (1998) 49-62

[26] E. Tronconi, Chemical Engineering Science 55 (2000) 6021-6036

[27] R.E. Hayes, Topics in Catalysis 37 (2006) 155-159

[28] D.L. Trimm, Catalysis Letters 46 (1997) 27-29

[29] H.Y. Lee, US 6548011 2003

[30] A. Orinak, Applied Surface Science 252 (2006) 7030-7033

[31] M. Jafelicci Jr, Journal of Non-Crystalline Solids 273 (2000) 36-40

[32] J.G.G. Goodwin Jr, Applied Catalysis A: General 281 (2005) 1-9

[33] Y.C. Yoo, Materials Letters 42 (2000) 362-366

[34] W.G. Sloof, Surface Science 496 (2002) 97-109

[35] J. Sainio, Applied Surface Science 252 (2005) 1076-1083

[36] F. Dorado, Applied Catalysis B: Environmental 73 (2007) 42-50

[37] E. Tronconi, Chem. Eng. Sci. 47 (1992) 2401

[38] E. Tronconi, Catal. Today 34 (1997) 421

[39] E. Tronconi, Catal. Today 52 (1999) 249

[40] A. Sassi, Topics in Catalysis 30/31 (2004) 267-272

[41] F.C. Galisteo, Applied Catalysis B: Environmental 59 (2005) 227-233

[42] J. Lahtinen, Journal of Chemical Physics 116 (2002) 9 3870-3874

[43] J. Mendez, Applied Surface Science 142 (1999) 152-158

[44] J.W. Geus, WO 99/05342 (1999)

[45] C.C. Li, Oxidation of Metals 61 (2004) 5/6 485-505

[46] A. Galerie, Materials and Corrosion 56 (2005) 6 389-392

[47] H.P. Martinz, Plansee GmbH, Hochtemperaturkorrosion, 1993, 42-43

[48] A. F. Holleman, Lehrbuch der Anorganischen Chemie, Walter de Gruyter, Berlin New York
1985, 1165

Chapter 7

7   Summary

7.1 SUMMARY

Stricter emission legislation requires constant improvement and development of catalytic systems for the emission reduction of internal combustion engines. Diesel and lean burn engines are generating pollutants which have to be reduced with different exhaust gas aftertreatment technologies. Three-way catalysts, oxidation catalysts, and particulate filters are available systems. The tasks of these modules are the reduction of harmful substances like, NO, CO, HC, PM. However, most modules are already in use and difficult to improve.

The main objective of the thesis was the introduction of sintered stainless steel hollow spheres as new support structures for an oxidation catalyst in diesel exhaust gas aftertreatment systems. Commercial available oxidation catalysts are based on ceramic or metal monoliths. Different stainless steels, Fe-Cr-Ni and Fe-Cr-Al, were compared to proof that hollow spheres are competitive to monolithic structures.

In chapter 3 the adhesion of oxide coatings, for the enlargement of surface and layer for the active component platinum, is investigated on sintered and rolled foils. The adhesion strength depends on pH, concentration of oxide solution, calcination temperature, and chemical composition. All these factors influence the interconnection between metal surface and coating. The surface morphology of sintered samples showed a rougher surface than rolled foils which creates more surface. Better adhesion was achieved for all tested washcoats on sintered support. A pH of 5 for a slurry of bohemite lead to the best adhesion performance. The weight loss measured according to DIN EN ISO 2409 induced by the grid-cut method could be controlled below 1% for sintered foils. The significant advantage of the bohemite, calcined coating exhibits small particles, was shown with SEM. Furthermore, XRD and adhesion test were used to show the advantage over silica, titania and zeolite β.

Chapter 4 describes a technique, neutron-tomography, which allows the non-destructive control of the quality and the manufacturing process of catalyst support structures. Phase contrast imaging increased the resolution of the images, thus allowing a detailed investigation of the geometrical properties for the single spheres. The hollow sphere structures had enhanced catalytic activity in the NO oxidation, which can only be utilized over densely packed structures. In the presence of open channels the activity was decreased and the generally higher pressure drop over these materials was compensated by the enhanced mass transfer.

In chapter 5, non-destructive investigations with computer- (X-ray) tomography and neutron tomography are combined for microscopic and macroscopic investigations of hollow sphere structures used as car exhaust catalysts. Determination of the wall and coating thickness of single spheres allow the improvement of the production procedure as well as the evaluation for quality control, done with computer-tomography. Further, the distribution of coke inside a real-size catalyst was studied with neutron tomography. The resulting distribution can lead to adjustments of gas flows to achieve homogeneous conditions.

In chapter 6 the oxidation of NO to NO_2 and CO to CO_2 is investigated in a tubular-flow model setup. The kinetic experiments have demonstrated that stainless steel hollow sphere structures are a promising alternative to monolithic catalysts as diesel emission catalysts for NO and CO oxidation. Similar catalytic activity was reached in the oxidation of NO to NO_2 and CO to CO_2 with hollow sphere supports compared to the traditional cordierite monolith supports. However caution is necessary in case of constant high temperature applications, which can lead to the migration of chromium from the support through the washcoat to the surface which causes a loss of activity for Fe-Cr-Ni alloys. Improvement of the stainless steel, changing the support structure to Fe-Cr-Al with low aluminum content, resulted in the growth of a protective alumina barrier layer during the pre-oxidation process. The metal hollow sphere structure made of Fe-Cr-Al can compete with the monolithic catalyst as support for NO and CO oxidation as Pt/Al_2O_3 diesel oxidation catalysts.

7.2 ZUSAMMENFASSUNG

Eine strengere Gesetzgebung zur Abgasminderung verlangt eine konstante Verbesserung und Entwicklung von katalytischen Systemen zur Emissionsverminderung von Verbrennungskraftmaschinen. Diesel- und Otto-Motoren generieren Abgase, die mit verschiedenen Technologien vermindert werden müssen. 3-Wege-Katalysatoren, Oxidationskatalysatoren und Partikelfilter sind einige dieser Systeme. Ihre Aufgabe ist die Umwandlung von schädlichen Substanzen wie NO, CO, HC oder PM in neutrale Substanzen. Jedoch sind die meisten dieser Systeme schon lange im Einsatz und die Technik ist meist ausgereift, wodurch eine Verbesserung erschwert wird.

Das Hauptziel dieser Arbeit ist der Einsatz von gesinterten Edelstahl-Hohlkugeln als neue Trägerstrukturen in einem Diesel-Oxidationskatalysator im Abgasnachbehandlungssystem. Verschiedene Stähle, Fe-Cr-Ni und Fe-Cr-Al, wurden verglichen, um die Wettbewerbsfähigkeit dieser Hohlkugelstrukturen gegenüber Monolithen zu beweisen.

In Kapitel 3 wird der Einfluss der Haftung von Oxidschichten zur Vergrößerung der Oberfläche und als Träger für die aktive Komponente Platin auf der Oberfläche von gesinterten und gewalzten Blechen untersucht. Dabei wurde die Abhängigkeit von verschiedenen Parametern wie pH-Wert, Konzentration der Lösung, Kalzinierungs-Temperatur und die Zusammensetzung der Oxidschicht erforscht. Alle diese Faktoren beeinflussen die Stärke der Verbindung zwischen Metalloberfläche und Beschichtung. Die Oberflächenstruktur der gesinterten Bleche weist größere Rauheit auf als die gewalzten Bleche, was zu einer größeren Oberfläche führt. Für alle getesteten Beschichtungen wurde eine bessere Haftung auf gesinterten Oberflächen erzielt. Das beste Ergebnis erzielte eine Böhmit-Beschichtung mit einem pH-Wert von 5. Damit konnte der Gewichtsverlust nach einem Test der Haftbarkeit, bestimmt nach DIN (DIN EN ISO 2409), unter 1% gehalten werden. Der entscheidende Vorteil der Böhmit-Beschichtung besteht darin, dass die kleinen Partikel zusammen eine feste Oberfläche bilden, wie mit SEM gezeigt werden

konnte. Darüber hinaus konnte mit XRD und dem Haftungstest gezeigt werden, dass eine Böhmit-Beschichtung Vorteile gegenüber Zeolith β, TiO_2 und SiO_2 hat.

Kapitel 4 beschreibt eine Messmethode, die Neutronen-Tomographie, mit der zerstörungsfrei die Qualität der Katalysatorstrukturen geprüft werden konnte. Eine Erhöhung des Phasenkontrastes erlaubte die Untersuchung der Zwischenräume in Kugelpackungen. Es stellte sich heraus, dass dicht gepackte Hohlkugelstrukturen eine höhere katalytische Aktivität in der Oxidation von NO haben. Der höhere Druckverlust bei Hohlkugelstrukturen fällt aufgrund des verbesserten Massentransports nicht ins Gewicht. Durch die Untersuchungen konnte die Packungsdichte erhöht werden; dies führte zu besseren Ergebnissen.

In Kapitel 5 wurde die Computer- (Röntgen) Tomographie durchgeführt, um die Vorteile beider Messprinzipien zu nutzen. Durch Neutronen-Tomographie wurde die Rußverteilung in einer makroskopischen Struktur (bereits eingesetzer Hohlkugel-Oxidationskatalysator) dargestellt. Dies kann zu einer Anpassung der Strömungsverhältnisse genutzt werden, um eine effizientere Rußabscheidung zu erreichen. Mit der Computer-Tomographie konnten die Wanddicke und die Beschichtungsdicke an einzelnen Hohlkugeln bestimmt werden.

In Kapitel 6 wird die Oxidation von NO und CO zu NO_2 und CO_2 am Modellgasprüfstand erforscht. Die katalytische Aktivität der Hohlkugelstrukturen ist vergleichbar mit keramischen Monolithen. Es konnte gezeigt werden, dass die gesinterten Metallkugeln eine viel versprechende Alternative darstellen. Jedoch ist Vorsicht geboten bei langen Hochtemperaturanwendungen, da bei Fe-Cr-Ni Stählen das Chrom an die Oberfläche wandern und damit die Aktivität senken kann. Die Wahl des Fe-Cr-Al Stahls mit einem niedrigen Anteil an Aluminium führt während der Vorbehandlung zur Ausbildung einer Aluminiumoxid-Schutzschicht. Gesinterte Hohlkugelstrukturen aus Fe-Cr-Al als Trägerstruktur eines Diesel-Oxidationskatalysators können mit monolithischen Strukturen konkurrieren.

Chapter 8

8   **Future Application**

8.1 FUTURE APPLICATION

The objective of this cooperative project was the development of a new exhaust gas system based on sintered metal hollow sphere structures.

To decide the geometry of a potential diesel oxidation catalyst for further investigations in an engine test bench a hollow sphere structure was designed. Dimensions and characteristics of the catalyst case in the test bench were taken into account. In the following paragraph the geometry of a demonstrator for an oxidation catalyst was calculated using the kinetic parameters described in chapter 6. The principle geometry demonstrator is shown in Figure 1.
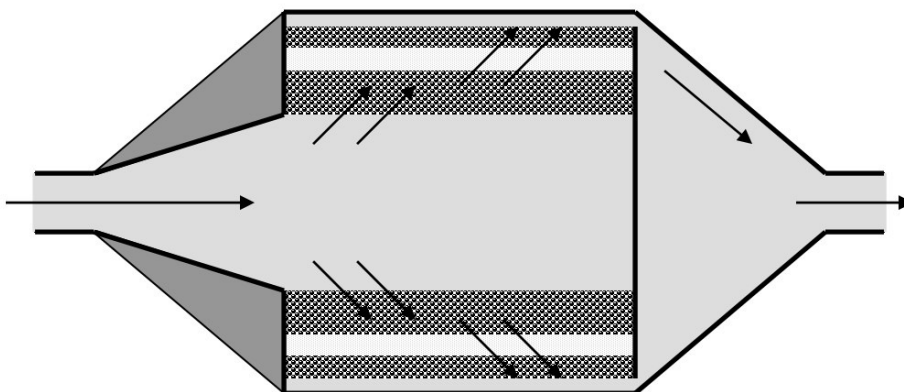

Figure 1: Scheme of demonstrator

The catalytic active hollow sphere structure consists of two hollow cylinders made of two half shells. The inner hollow cylinder has an inner diameter of 60 mm and 100 mm for the outer diameter. The bigger hollow cylinder has an inner diameter of 120 mm and an outer diameter of 140 mm. The gap between both cylinders was filled with a commercially available permeable fiber mat in order to remove particles. The gas flow enters the device through a 60 mm diameter inlet tube and the radial distribution through the hollow sphere structures occurred from inside to the outside.

97

For the modeling of the demonstrator the following formula was used:

Equation 1:

$$X = 1 - e^{-\frac{V \cdot k \cdot c_{NO_0}}{F_{NO_0}}}$$

This equation is based on a first order reaction using integral analysis for the rate. X indicates the NO conversion [%], V the educt flow [mol/s], c_{NO0} the initial NO concentration [mol/l], k the rate constant [1/s] and V the catalyst volume [1]. Radial gradients of temperature, concentration and reaction rate were neglected in the tubular flow reactor. Using this equation the catalyst volume and for the know geometry the length of the catalyst bed can be calculate for the required conversion level.

The rate constants described in chapter 6 and the reaction conditions in the test bench are summarized in Table 1.

Table 1: Parameters for modeling

	value	unit
Rate constant k	166	1/s
Molar flow F	3.7×10^{-3}	Mol/s
Concentration c	$4.2 \times 10{-6}$	Mol/l
Conversion NO		%
Volume of catalyst		L
Length of catalyst		Cm

An optimal diameter for the application of the oxidation catalyst in cars is 6 mm. Therefore, both diameters, 3 mm and 6 mm, were included in the model. The diameter influences the total surface of hollow spheres and the surface ratio of 3 mm: 6 mm is 2:1.

The conversion calculated as function of the length of the catalyst for 3 and 6 mm spheres is shown in Figure 2.
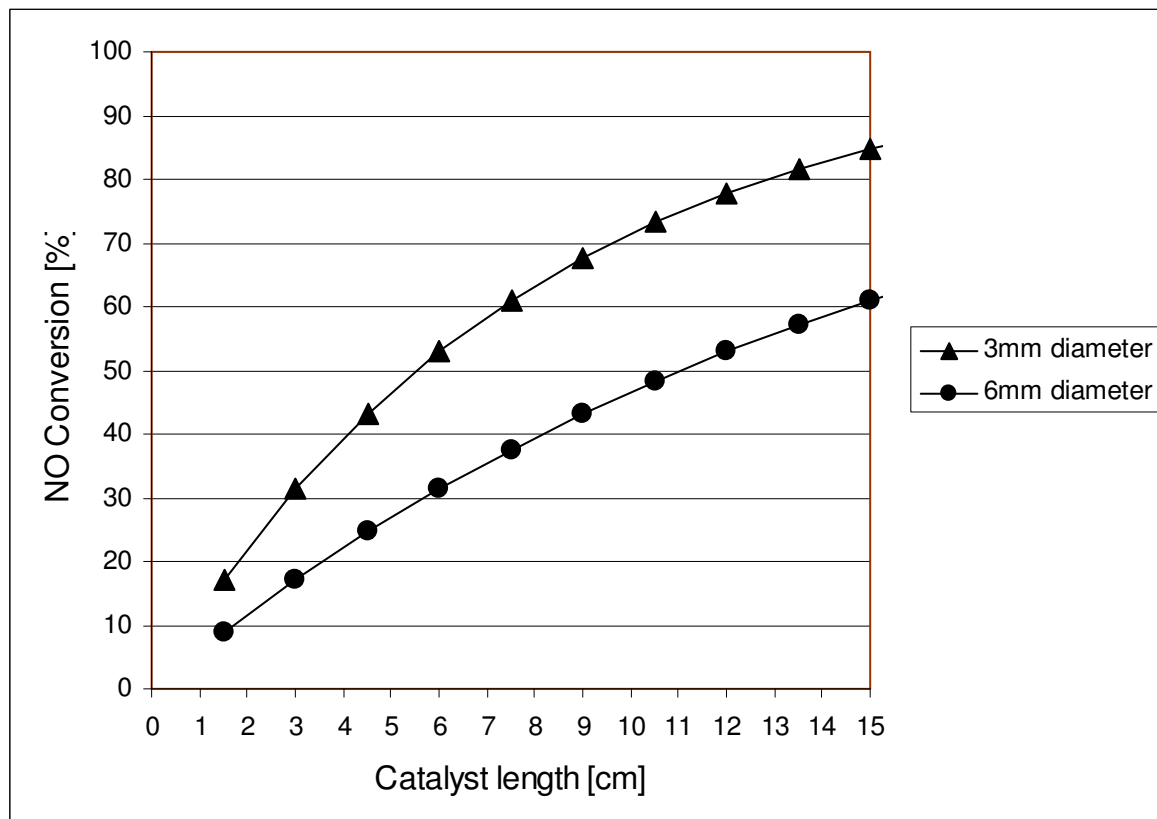

Figure 2: NO conversion over catalyst length for 3 mm and 6 mm hollow spheres

The purpose of the oxidation catalyst is to provide a NO_2 conversion of 50% to enhance the NOx reduction and to supply an oxidant for the regeneration of the particulates in the DPF. From the model a catalyst length of 6 cm was predicted to reach 50 % conversion. In comparison with existing oxidation catalysts (25 cm length), the length can be reduced at the same calculated NO conversion abilities. The promising result of the project will be applied in a demonstrator to test the efficiency under real conditions and the oxidation catalyst can be combined with a particulate filter system based on a hollow sphere structure.

8.2 REFERENCES

[1] G. Emig, E. Klemm, in Technische Chemie, Springer, Berlin (2005)

CURRICULUM VITAE

Wolfgang Kaltner was born in München, Germany, on 17th July 1978. After finishing high school in Dachau in 1998 and subsequent civil service, he started his chemical engineering studies at the Technische Universität München in 1999. He finished his studies in 2004 after writing his Diploma Thesis entitled "Selective Hydrogenation of nitriles to amines and characterization of the supported metal catalysts", which was performed under the supervision of Prof. J.A. Lercher at Technische Universität München. Afterwards he stayed at the Chair 2 of Chemical Technology (TC2) to start the research on hollow sphere structures for the emission limitation of internal combustion engines.

POSTER PRESENTATIONS

1. 40. Jahrestreffen Deutscher Katalytiker, 14. – 16.03.2007 in Weimar

   W. Kaltner, K. Lorenz, A. Jentys, J.A. Lercher, poster

2. First FRM II user meeting, 30.10.2007 in Garching

   W. Kaltner, K. Lorenz, A. Jentys, B. Schillinger, J.A. Lercher, poster

3. 41. Jahrestreffen Deutscher Katalytiker, 27. – 29.02.2008 in Weimar

   W. Kaltner, K. Lorenz, A. Jentys, J.A. Lercher, poster